The non-coding RNA miR-17~92 is a central mediator of T cell activation

Authors

Marianne Dölz[1, 2], John D. Gagnon[3, 4, 5], Mara Kornete[1, 6], Romina Marone[1, 2], Glenn Bantug[1], Robin Kageyama[3, 4], Christoph Hess[1, 7], K. Mark Ansel[3,4], Denis Seyres[1, 2], Julien Roux[1,8] and Lukas T. Jeker[1, 2]*

Affiliations

1 Department of Biomedicine, Basel University Hospital and University of Basel, Hebelstrasse 20, CH-4031 Basel, Switzerland.

2 Transplantation Immunology & Nephrology, Basel University Hospital, Petersgraben 4, CH-4031 Basel, Switzerland

3 Department of Microbiology and Immunology, University of California, San Francisco, California 94143, USA

4 Sandler Asthma Basic Research Center, University of California, San Francisco, California 94143, USA

5 Present address: ArsenalBio, 571 Eccles Ave, South San Francisco, CA 94080, USA

6 Present address: Département Formation et Recherche CHUV, Lausanne, Switzerland

7 Department of Medicine – CITIID, University of Cambridge, Puddicombe Way, Cambridge CB2 0AW, United Kingdom

8 Swiss Institute of Bioinformatics, Basel, Switzerland

* Corresponding author and lead contact: lukas.jeker@unibas.ch

Summary

T cell activation is paramount for productive adaptive immune responses. CD28 is a key clinically targeted immunoregulatory receptor because it provides the prototypical costimulatory signal required for T cell activation. Therefore, a precise understanding of the molecular consequences of CD28 costimulation has direct therapeutic relevance. Here, we uncover that the microRNA cluster miR-17~92 is part of the molecular program triggered by CD28 costimulation and hence T cell activation. Combining genetics, transcriptomics, bioinformatics and biochemical miRNA:mRNA interaction maps we demonstrate that transgenic miR-17~92 can cell-intrinsically largely overcome defects caused by CD28-deficiency. miR-17~92 promotes transcription of a proinflammatory gene signature by enhancing the calcineurin/NFAT pathway. miR-17~92 binds to and represses a network of genes including several negative regulators of T cell activation. Finally, CD28-deficient T cells exhibit derepressed miR-17~92 target genes during activation, demonstrating that this non-coding RNA is required to shape the transcriptome. Thus, we propose that miR-17~92 constitutes a central mediator for T cell activation, integrating signals by the TCR and CD28 costimulation. In this model miR-17~92 facilitates T cell activation by dampening the brakes that prevent T cell activation.

Keywords

T cell activation, non-coding RNA, microRNA, posttranscriptional gene regulation, miR-17~92, CD28 costimulation

Introduction

T cells are paramount to protect mammals from infections and tumors. T cell activation, a key event for adaptive immunity, relies on two signals: T cell receptor (TCR) stimulation as well as costimulation by specialized receptors. While the TCR signal provides specificity, costimulation by antigen presenting cells (APCs) provides quantitiative and qualitative support for T cell activation [1,2]. One of the best studied and prototypical costimulatory molecules is CD28. It promotes multiple processes required for T cell biology such as T cell activation, proliferation, survival, metabolic adaptation and Interleukin-2 (IL-2) production [2,3]. These form the basis for clonal expansion and T cell differentiation into a variety of effector T cells that are necessary to mount effective immune responses. Recent data further demonstrates that CD28 expression is not only required for T cell priming but also days later for effector $CD4^+$ T cell responses during infection [4].

Due to its centrality for T cell and immune responses more generally, CD28 is an important target in therapeutic immunology [2,5,6]. CD28 blockade by CTLA4-Ig is clinically used to prevent renal allograft rejection and to treat rheumatic disease [2]. In contrast, vaccine adjuvants induce activation of innate immune cells to express ligands that trigger costimulatory molecules on T cells. Furthermore, immune-activating CTLA-4 blocking antibodies represent the foundation of cancer immunotherapy [7] and CD28 is required for cancer immunotherapy with PD-1 blocking antibodies [8-10]. Finally, CD28 intracellular signaling domains can provide the required costimulatory signal in 2nd and 3rd generation chimeric antigen receptor (CAR) T cell constructs for adoptive cellular therapies [11]. Thus, CD28 is a key clinically relevant immunoregulatory receptor and a precise understanding of molecular events induced by CD28 costimulation has direct therapeutic relevance. However, despite intense research, the understanding of the molecular consequences of CD28 costimulation remains incomplete [2]. CD28 costimulation acts through pleiotropic effects; it promotes the phosphatidylinositol 3-kinase (PI3K) pathway, amplifies the TCR signal, stabilizes the transcriptome induced by TCR stimulation and enhances calcineurin/NFAT signaling [2,3,12]. Collectively, CD28 stimulation ultimately leads to transcriptional changes mediated by the transcription factors (TF) NF-κB, AP-1 and NFAT [2]. In addition, CD28 also acts through many non-transcriptional mechanisms such as mRNA stabilization and altered mRNA splicing [2]. Thus, due to the complexity of CD28 costimulation, substantial controversy remains about the importance of various molecular mechanisms and the relative importance of quantitative versus qualitative CD28-mediated signals [1-3,5].

Since a protein-centric view prevailed in most studies, here we investigated the role of the microRNA cluster miR-17~92, a non-coding RNA, in CD28 costimulation and T cell activation. MicroRNAs (miRNA) are arguably the best studied class of non-coding genes.

88 These short RNA molecules of ~22nt length are highly conserved gene repressors that mainly
89 act through base pairing with the 3' untranslated region (UTR) of target RNAs resulting in their
90 decreased abundance and/or translational inhibition [13]. Together with TFs, miRNAs are the
91 most important trans-regulators of gene expression, regulating most mRNAs [14]. Target RNAs
92 can be bound by multiple miRNAs and individual miRNAs can bind to and repress multiple
93 genes, often genes found in the same pathway [13]. Canonical base-pairing is largely determined
94 by miRNA nucleotide positions 2-7, called the "seed" region [14] but non-canonical miRNA
95 targeting is widespread and can be equally effective [15,16]. The interaction of a miRNA and its
96 target mostly results in mild gene repression, often only reducing protein concentration by less
97 than 2-fold. Nevertheless, miRNA-mediated gene regulation is highly consequential for T cell
98 differentiation and function [13,17-19].
99 We noticed that key functions attributed to CD28 such as T cell proliferation, survival and T_{FH}
100 differentiation are also regulated by miR-17~92. miR-17~92, a polycistronic transcript induced
101 by CD28 costimulation [20], gets processed into 6 mature miRNAs representing 4 different seed
102 families [17]. Much like CD28, miR-17∼92 promotes T cell proliferation, survival and
103 differentiation [19,21]. Moreover, T cell-specific miR-17∼92-deficiency results in severely
104 impaired T_{FH} differentiation and impaired GC formation [22,23], reminiscent of impaired GC
105 formation observed in CD28-deficient mice [24]. On the contrary, miR-17∼92 overexpression
106 results in a systemic lupus-like syndrome with increased GC formation and autoantibody
107 production [21] most likely due to enhanced T_{FH} generation [22,23].
108 Here, we show that miR-17∼92 was necessary to mediate part of the molecular changes
109 induced by CD28 costimulation and its forced expression was sufficient to restore an important
110 fraction of the impaired transcriptional regulation and function of CD28-deficiency in murine
111 $CD4^+$ T cells. We used transcriptome analysis, computational predictions and biochemical
112 miRNA/target RNA interaction maps to define a high confidence set of 68 empirically validated
113 direct miR-17∼92 target genes in T cells. Pathway analysis revealed that miR-17∼92 promoted
114 expression of NFAT-regulated genes. Pharmacologic experiments using the calcineurin
115 inhibitor cyclosporin A (CyA) confirmed that miR-17∼92 promoted the calcineurin/NFAT
116 pathway. Our results identify miR-17∼92 as an important mediator of CD28-costimulation
117 induced T cell activation that promotes key activating pathways. We propose that miR-17∼92
118 represses multiple inhibitory proteins that restrain T cells from becoming activated.
119

120 **Results**

121 **miR-17~92 regulates T cell proliferation and Interleukin-2 production**

122 In order to further investigate the connection between CD28 and miR-17~92, we analyzed the
123 consequences of T cell-specific loss and gain of miR-17~92 on key processes regulated by
124 CD28. We compared samples from mice that lack miR-17~92 in T cells (CD4cre.miR-
125 17~92$^{lox/lox}$, designated T$^{1792\Delta/\Delta}$ hereafter), wildtype (wt) mice and mice overexpressing miR-
126 17~92 in T cells (CD4cre.Rosa26^{lox}STOP^{lox}CAG-miR-17~92Tg, designated T$^{1792tg/tg}$
127 hereafter). Confirming previous findings, we showed that miR-17~92 promotes T cell
128 proliferation (Fig. 1a) [22,23,25]. In addition, in comparison to wt T cells, production of the classic
129 CD28-dependent gene interleukin-2 (IL-2) was impaired in T$^{1792\Delta/\Delta}$ T cells and increased in
130 T$^{1792tg/tg}$ T cells. Intracellular IL-2 and IL-2 secretion correlated with the miR-17~92 genotype
131 (Fig. 1b, c). Thus, miR-17~92-deficiency was reminiscent of phenotypes observed in CD28-
132 deficient mice. In contrast, transgenic miR-17~92 appeared to enhance T cell
133 activation/costimulation. Thus, the data suggested that the non-coding RNA miR-17~92
134 exerted a dose-dependent regulation of CD4$^+$ T cell proliferation, IL-2 production, and more
135 complex biologic functions such as T_{FH} differentiation[22,23], all of which are known to be CD28-
136 dependent.

137

138 **Transgenic miR-17~92 enables T cell activation of CD28-deficient T cells in vitro**

139 Since miR-17~92 expression is induced in a CD28-dependent manner during T cell activation
140 [20], we hypothesized that miR-17~92 could be a downstream mediator of CD28 costimulation.
141 To test this hypothesis we crossed B6.CD28$^{-/-}$ (CD28$^{-/-}$) mice [26] with T$^{1792tg/tg}$ mice, resulting in
142 B6.CD28$^{-/-}$.CD4cre.Rosa26^{lox}STOP^{lox}CAG-miR-17~92Tg, designated "rescue" hereafter. T
143 cells in these mice lack CD28 but constitutively express transgenic miR-17~92. If miR-17~92
144 physiologically transmitted signals induced by CD28 then we expected that transgenic miR-
145 17~92 expression could restore some of the CD28 defects. First, we investigated how "rescue"
146 cells behaved in vitro. We compared wt, CD28$^{-/-}$ and "rescue" naïve CD4$^+$ T cells stimulated
147 with plate-bound anti-CD3 mAb alone to mimic signal 1 or a combination of anti-CD3 and
148 anti-CD28 mAb to mimic combined signals 1 and 2. As expected, wt cells blasted (Fig. 2a) and
149 increased proliferation (Fig. 2b) in response to costimulation compared to anti-CD3 stimulation
150 alone. Compared to wt cells, CD28$^{-/-}$ T cells showed reduced size and proliferation and were
151 unable to respond to anti-CD28 stimulation (Fig. 2a,b). In contrast, "rescue" T cells stimulated
152 with anti-CD3 alone or combined anti-CD3/anti-CD28 blasted and proliferated like wt T cells
153 fully stimulated with anti-CD3 and anti-CD28 mAb (Fig. 2a, b). Since IL-2 production is a
154 major consequence of CD28 costimulation and miR-17~92 correlated strongly with IL-2
155 production (Fig. 1b,c) we analyzed this cytokine next. As with blasting or proliferation, CD28-

156 deficient T cells produced less IL-2 but "rescue" T cells produced even supraphysiologic
157 amounts of IL-2 (Fig. 2c). Thus, transgenic miR-17~92 was sufficient to replace CD28 for
158 three major costimulation-dependent processes and IL-2 was very sensitive to miR-17~92
159 expression. Since these experiments were carried out in the presence of exogenous IL-2 it is
160 unlikely that increased blasting and proliferation were a consequence of increased IL-2 but
161 rather reflected a cell-intrinsic effect.
162 Next we turned our attention to surface markers whose expression is either TCR- or CD28-
163 dependent. The early activation marker CD69 is rapidly upregulated during T cell activation
164 and reflects TCR signaling strength [27]. As a second marker we used the high affinity IL-2
165 receptor alpha subunit CD25, a well-known CD28-dependent gene. The relative number of
166 cells that expressed CD69 and CD25 (Fig. 2d) and CD69 expression per cell (Fig. 2e) was
167 comparable for all genotypes, as predicted for a TCR-dependent marker. In contrast, the signal
168 intensity of CD25 was clearly CD28-dependent. Wildtype T cells increased CD25 MFI after
169 CD28 costimulation while $CD28^{-/-}$ T cells displayed lower CD25 MFI than wt cells and were
170 unable to respond to CD28 stimulation, reflecting defective CD28 signaling. In contrast, CD25
171 expression was fully restored in "rescue" T cells, even after anti-CD3 stimulation alone (Fig.
172 2f). Finally, CD44 expression was also highly CD28-dependent. In concert with the other
173 CD28-dependent parameters (blasting, proliferation, IL-2 and CD25), wt T cells responded to
174 CD28 ligation with CD44 expression but $CD28^{-/-}$ cells lacked CD44 upregulation. In contrast,
175 the frequency of $CD44^{hi}CD62L^{lo}$ "rescue" T cells was at least comparable to fully costimulated
176 (anti-CD3/anti-CD28) wt T cells (Fig. 2g). Thus, the miR-17~92 transgene appeared to
177 efficiently replace CD28 function in vitro.
178
179 **Transgenic miR-17~92 enables T cell activation of CD28-deficient T cells in vivo**
180 Next we investigated whether transgenic miR-17~92 could also substitute CD28 function in
181 vivo. $CD28^{-/-}$ mice display a severe defect in T_{FH} development and GC formation [24,26,28,29].
182 Therefore, we infected wt, $CD28^{-/-}$ and "rescue" mice with lymphocytic choriomeningitis virus
183 (LCMV) Armstrong to induce an acute viral infection leading to T_H1 and T_{FH} differentiation as
184 well as GC B cell formation. Confirming previous literature, we found severely impaired CD44
185 upregulation, T_{FH} differentiation and GC B cell formation in $CD28^{-/-}$ mice compared to wt
186 littermates (Fig. 3a-d). In contrast, all these parameters were restored in "rescue" mice (Fig. 3a-
187 d). This is remarkable given the complexity of T_{FH} differentiation [30]. In addition, rescued T cells
188 not only phenotypically resembled T_{FH} cells through their expression of CXCR5, PD-1, Bcl-6
189 and ICOS (Fig. 3b,c) but they were functional because they induced GC B cell formation which
190 reflects T_{FH}/B cell crosstalk. Furthermore, the spleen of infected "rescue" mice, but not $CD28^{-}$
191 $^{/-}$ mice, featured organized GCs containing $GL7^{+}$ B cells and $CD4^{+}$ T cells (Fig. 3e)

192 demonstrating restoration of another hallmark defect found in CD28$^{-/-}$ mice [24]. Finally, we
193 analyzed T_H1 responses and found that transgenic miR-17~92 restored the defect in T_H1
194 differentiation observed in CD28$^{-/-}$ mice (Fig. 3f,g). We noticed that fewer CD28$^{-/-}$ cells
195 expressed Tbx21 compared to wt cells (Fig. 3f). However, some of those cells that did express
196 Tbx21 co-expressed IFNγ, even in CD28$^{-/-}$ cells. Analyzing the ratio of Tbx21^{+}IFNγ^{+}/Tbx21^{+}
197 T cells confirmed that the missing costimulatory signal mainly resulted in defective Tbx21
198 induction rather than IFNγ production (Fig. 3h). These results suggest that the CD28$^{-/-}$ defect
199 acts during T cell activation, i.e. before T_H1 differentiation. Accordingly, the miR-17~92
200 transgene appears to restore T cell activation signals.
201 T$^{1792tg/tg}$ T cells displayed increased proliferation and IL-2 secretion compared to wt cells (Fig.
202 1) and intracellular IL-2 was not only restored but even higher in "rescue" T cells than wt T
203 cells (Fig. 2c), suggesting that the effect of miR-17~92 depended on its abundance. Therefore,
204 we investigated the effect of a single copy of the miR-17~92 transgene in CD28$^{-/-}$ cells. In
205 addition, we directly compared the effect of the miR-17~92 transgene in CD28-deficient and
206 CD28-sufficient T cells in vivo to test if CD28 triggering and the miR-17~92 transgene were
207 additive. To this end, we infected CD28$^{-/-}$, T$^{1792\Delta/\Delta}$, wt, het rescue, rescue and T$^{1792tg/tg}$ mice with
208 LCMV Armstrong. "het rescue" were CD28$^{-/-}$ that only carried one copy of the miR-17~92 Tg
209 while "rescue" mice were the rescue mice used above (Figs. 2, 3) with two copies of the miR-
210 17~92 transgene. The relative number of CD44^{+} T cells was lowest in CD28$^{-/-}$ and highest in
211 T$^{1792tg/tg}$ mice (Suppl. Fig. 1a). We observed a similar but less pronounced effect for T_{FH}, GC B
212 cell formation and T_H1 differentiation (Suppl. Fig. 1b-g). CD28$^{-/-}$ and T$^{1792\Delta/\Delta}$ mice exhibited a
213 comparable defect but unlike CD44, T$^{1792tg/tg}$ did not increase T_{FH}, GC B cell formation and T_H1
214 differentiation compared to wt mice. In summary, a single copy of the miR-17~92 transgene
215 partially restored several parameters while two transgene copies further increased the rescue
216 effect. The presence of CD28 and two transgene copies further increased IL-2 and T_H1
217 formation. Thus, miR-17~92-mediated gene regulation is very sensitive to precise miR-17~92
218 expression in vivo.
219 To exclude altered viral clearance as a confounding factor we verified that wt, CD28$^{-/-}$ and
220 "rescue" mice normally cleared LCMV. Viral load was below detection level in plaque assays
221 (data not shown). This is consistent with literature that LCMV clearance at this time point is
222 CD8-mediated and CD28-independent. In summary, we found an unexpectedly complete
223 restoration of CD28 costimulatory function and T cell activation exerted by transgenic miR-
224 17~92 expression in vitro as well as in vivo.
225
226
227

228 **Restoration of T cell activation of CD28-deficient T cells by miR-17~92 is cell intrinsic**
229 Although CD28's main function is on T cells, we sought to formally test whether the miR-
230 17~92-mediated rescue effect was cell intrinsic. We crossed MHC class II restricted $CD4^+$
231 TCR transgenic mice specific for LCMV (SMARTA; $V\alpha2^+V\beta8.3^+$) to wt, $CD28^{-/-}$ and "rescue"
232 mice. We adoptively transferred (AT) naïve $CD4^+$ T cells to $CD28^{-/-}$ host mice followed by
233 acute LCMV infection. Eight days post infection we isolated spleen, mesenteric and peripheral
234 lymph nodes (LN). In all three organs the frequency and absolute number of $V\alpha2^+V\beta8.3^+$
235 $CD28^{-/-}$ cells was strongly reduced compared to $V\alpha2^+V\beta8.3^+$ $CD28^{wt/wt}$ cells. In contrast, the
236 miR-17~92 transgene restored relative and absolute numbers of $V\alpha2^+V\beta8.3^+$ $CD28^{-/-}$ T cells
237 (Fig. 4a and Suppl. Fig. 2a, b). Furthermore, among $V\alpha2^+V\beta8.3^+$ T cells, fewer $CD28^{-/-}$ cells
238 upregulated CD44 than in wt cells, a defect that was entirely restored in rescue cells (Fig. 4b
239 and Suppl. Fig. 2c, d). Thus, these data unequivocally demonstrate that transgenic miR-17~92
240 cell intrinsically compensated for CD28-deficiency. Collectively, we conclude that the non-
241 coding RNA miR-17~92 can restore costimulatory function in CD28-deficient T cells.
242
243 **miR-17~92 shapes the transcriptome after $CD4^+$ T cell activation**
244 To unravel the molecular mechanism underlying miR-17~92-mediated function during T cell
245 activation we performed RNA-sequencing on naïve and in vitro activated (24h and 48h) $CD4^+$
246 T cells from $T^{1792\Delta/\Delta}$, wt and $T^{1792tg/tg}$ mice. Principal component analysis (PCA) revealed that
247 the transcriptomes of naïve T cells from all three genotypes were very similar (Fig. 5a, 0h). T
248 cell activation induced major changes in gene expression (PC1, 56.7% of variance explained
249 and PC2, 14% of variance explained) and also made the genotypes separate at 24h and even
250 more clearly at 48h after activation (Fig. 5a; Suppl. Fig. 3a) (PC1 and PC3, 7.2% of variance
251 explained). Since miRNAs often repress individual genes only mildly [14], we compared the most
252 extreme genotypes, i.e. $T^{1792\Delta/\Delta}$ to $T^{1792tg/tg}$ to increase the power of differential gene expression
253 analysis, at each time point. At a false discovery rate (FDR) of 1%, the number of differentially
254 expressed genes (DEG) increased over time (830 genes up-regulated and 789 genes down-
255 regulated at 0h, 2,493 up and 2,370 down at 24h, and 3,173 up and 3,242 down at 48h).
256 Unsupervised hierarchical clustering of DEG 24h after activation revealed a nuanced pattern of
257 gene clusters (Fig. 5b). As expected from the PCA (Fig. 5a), gene expression across genotypes
258 was very similar in naïve T cells and the magnitude of expression differences increased after
259 activation (Fig. 5b). According to their expression profile, we defined 4 different groups of
260 genes (Fig. 5b): cluster I genes were induced over time and enhanced in $T^{1792tg/tg}$ compared to
261 wt but reduced or delayed in $T^{1792\Delta/\Delta}$. Cluster II genes decreased with time and miR-17~92
262 supported their repression. Overall cluster III gene expression increased after activation but
263 expression per time point inversely correlated with the genotype ($T^{1792\Delta/\Delta} > T^{1792tg/tg}$). Thus,

264 miR-17~92 limited initial or final maximal expression of genes in this group despite their
265 induction with time. Finally, genes displaying the most obvious inverse correlation with the
266 genotype were grouped in clusters IVa and IVb.
267 To analyze gene regulation modalities of the different clusters, we used exon-intron split
268 analysis (EISA) to discriminate between transcriptional versus posttranscriptional regulation
269 [31]. In addition, we employed computational target gene predictions from the Targetscan ("TS")
270 database [32] and used a dataset of biochemically detected direct miRNA:mRNA interactions in
271 T cells defined by Argonaute 2 high-throughput sequencing of RNA isolated by crosslinking
272 immunoprecipitation ("AHC") [33]. For each gene we quantified the read coverage on TS seed
273 matches for each of the miR-17~92 cluster seed families. These predictors of transcriptional
274 ("DE intron") and posttranscriptional regulation ("TS", "AHC"), annotated on the heatmap
275 (Fig. 5b) revealed genes whose expression increased over time and positively correlated with
276 the miR-17~92 genotype. They were enriched for transcriptional regulation and displayed few
277 TS sites or AHC reads (Fig. 5b, box I). Thus, cluster I was mainly induced by increased gene
278 transcription and miR-17~92 promoted this transcriptional activity. Examples include *Cd44*,
279 *IL-21*, *Tbx21* and *IFNγ* (Fig. 5c). In contrast, genes from clusters IVa and IVb (Fig. 5b, boxes
280 IVa, IVb) displayed a consistent and colinear reduction of expression levels across genotypes
281 that inversely correlated with miR-17~92 dosage ($T^{1792\Delta/\Delta}$ > wt > $T^{1792tg/tg}$) at 24h and 48h.
282 Importantly, these clusters contained few transcriptionally regulated genes but were enriched
283 for TS sites (p-value=0.001037; Fisher test) and experimentally determined AHC reads (p-
284 value=0.003598; Fisher test) (Fig. 5b). Thus, these clusters were mainly regulated
285 posttranscriptionally and likely constituted direct miR-17~92 target genes.
286 To further characterize direct miR-17~92 target genes we focused on naïve T cells and the 24h
287 time point since indirect effects likely increased after this time point. To visualize the effect of
288 individual miR-17~92 cluster miRNAs on their target genes we compared expression of genes
289 identified by TS and with >5 AHC reads for each miRNA seed family to all genes without any
290 seed match for that family. As illustrated by the miR-17 seed family, the miR-17~92 transgene
291 repressed miR-17 target genes in naïve T cells (Fig. 5d, left panel) but absence of miR-17~92
292 had no effect on the expression of miR-17 target genes (Fig. 5d, right panel). In contrast, after
293 T cell activation miR-17 target genes were repressed in $T^{1792tg/tg}$ T cells (Fig. 5e, left panel) and
294 derepressed in $T^{1792\Delta/\Delta}$ T cells (Fig. 5e, right panel). Similar effects were observed for all seed
295 families although to a lesser extent for the miR-18 seed family (Suppl. Fig. 3b, c). We defined
296 genes as empirically validated miR-17~92 targets if they fulfilled the following criteria: i)
297 significant derepression in $T^{1792\Delta/\Delta}$ vs wt and significant repression in $T^{1792tg/tg}$ vs wt at 24h ii)
298 predicted TS match iii) >5 AHC reads and iv) posttranscriptional regulation based on EISA.
299 Applying these criteria across the 4 seed families from miR-17~92 defined a set of 68

300 empirically supported direct miR-17~92 target genes (Suppl. Table 1). These genes included
301 previously described miR-17~92 targets validated in T cells, such as *Phlpp2* [23] and *Cyld,*
302 validated in B cells [34] (Fig. 5f). In addition, this approach identified many less studied genes
303 (e.g. *Rcan3, Nrbp1, Rnf38 and Rnf167*) as miR-17~92 targets in T cells (Fig. 5f). Notably,
304 several of the target genes negatively regulate pathways important for T cell activation. For
305 instance *Phlpp2* is a PI3K inhibitor [23], *Cyld* is a NF-κB inhibitor [35] and *Rcan3* a putative
306 calcineurin inhibitor [36] (Fig. 5f). Since miR-17~92 has not been reported to regulate calcineurin
307 signaling in T cells, we validated the *Rcan3* RNA-Seq data by qPCR on independent biologic
308 replicates (Fig. 5g). Moreover, its 3'UTR contains a conserved miR-17-5p 8mer binding site
309 and AHC confirmed a single discrete peak at this site, evidence for a direct interaction of a
310 miRNA with the *Rcan3* 3'UTR in primary T cells (Fig. 5h and [15,33]). Together, these data
311 empirically validate *Rcan3* as a miR-17 target in T cells.
312 Thus, using a combination of experimentally validated differential gene expression ($T^{1792\Delta/\Delta}$,
313 wt and $T^{1792tg/tg}$ T cells), evidence of posttranscriptional gene regulation and biochemical
314 detection of miRNA binding we defined a high confidence set of miR-17~92 target genes in T
315 cells. miR-17~92 became functionally relevant after T cell activation and shaped the
316 transcriptome in intricate ways. Our data demonstrates that miR-17~92 can promote and inhibit
317 gene expression. miR-17~92-mediated transcriptional consequences are most likely indirectly
318 mediated through posttranscriptional gene regulation. In addition, direct inhibition can enhance
319 gene silencing or dampen expression of induced genes. Thus, miR-17~92-mediated gene
320 repression is very powerful to shape the T cell transcriptome during T cell activation.
321
322 **miR-17~92 promotes the calcineurin/NFAT pathway in $CD4^+$ T cells**
323 To identify which molecular pathways were regulated by miR-17~92, we analyzed curated
324 gene sets enriched for differentially expressed genes between $T^{1792tg/tg}$ and $T^{1792\Delta/\Delta}$. At 24h, the
325 gene sets with the highest statistical significance and largest average fold change were related
326 to cytokines, inflammation and T cell differentiation (Suppl. Fig. 4a) while at 48h many
327 metabolic pathways were altered (Suppl. Fig. 4b). Next, we performed enrichment analysis on
328 DoRothEA regulons [37] to identify TF activity that could explain the regulated pathways.
329 Regulons were defined using any existing interaction with a particular TF. At 24h, the five most
330 significantly enriched TF regulons with the highest fold change contained two NFAT members
331 (NFATC2, NFATC3) as well as RELA, NF-κB1 and GATA3 (Fig. 6a). Since NFAT TFs are
332 important for T cell activation and differentiation (including T_{FH} differentiation [38]) but miR-
333 17~92 is not known to promote NFAT activity in T cells, we focused on the calcineurin/NFAT
334 axis. Genes belonging to regulons NFATC2 and NFATC3 include many T cell lineage-defining
335 TFs, cytokines and cytokine receptors and most of them – including *IL-21*, *Tbx21* and *IFNγ*

336 (Fig. 5c) - were highly regulated by miR-17~92 (Fig. 6b). This confirmed that miR-17~92
337 constitutes a central regulator of T cell activation and suggested that transgenic miR-17~92
338 enhanced canonical pathways that resulted in functional substitution of CD28 for differentiation
339 of T_{FH} and T_H1 in vivo (Fig. 3). Since miR-17~92 promoted expression of signature TF and
340 cytokines defining multiple T cell subsets, we tested if miR-17~92 more generally could
341 replace CD28. To this end we differentiated T_H1, T_H17 and iTreg cells in vitro. We confirmed
342 that also in this setup transgenic miR-17~92 was sufficient to compensate for the absence of
343 CD28 and functionally corrected the defects of $CD28^{-/-}$ T cells to differentiate into all 3 subsets
344 (Suppl. Fig. 5).
345 While miR-17~92 predominantly promoted inflammatory pathways at 24h, at 48h several
346 metabolic pathways were regulated by miR-17~92 (Suppl. Fig. 4a, b). Thus, we hypothesized
347 that initial transcriptional changes could lead to altered metabolism. It was recently shown that
348 cell cycle entry of quiescent T cells was controlled by store operated Ca^{2+} entry (SOCE) and
349 calcineurin/NFAT through control of glycolysis and oxidative phosphorylation [39]. Therefore,
350 we analyzed T cell metabolism in naïve and activated $T^{1792\Delta/\Delta}$, wt and $T^{1792tg/tg}$ T cells. In line
351 with the trancriptome results (Fig. 5), metabolic flux analysis demonstrated comparable
352 glycolytic and respiratory activity of naïve T cells in $T^{1792\Delta/\Delta}$, wt and $T^{1792tg/tg}$ T cells (Suppl.
353 Fig. 6a, b). In contrast, 48h after activation, glycolytic and respiratory activity positively
354 correlated with the miR-17~92 genotype (Suppl. Fig. 6c, d). Furthermore, genes associated
355 with the TCA cycle and respiratory electron transport positively correlated with miR-17~92 at
356 48h but not before, supporting the notion that miR-17~92 indirectly promoted this metabolic
357 activity (Suppl. Fig. 6e).
358 Since transcriptome analysis identified calcineurin/NFAT as a key pathway promoted by miR-
359 17~92 (Fig. 6a, b), we designed experiments to functionally validate this increased activity.
360 We activated wt, $CD28^{-/-}$ and "rescue" T cells in the presence of cyclosporin A (CyA), a direct
361 pharmacological calcineurin inhibitor (CNI) and quantified CD69/CD25 expression. Compared
362 to wt cells, $CD28^{-/-}$ cells were 4-fold more sensitive to CyA (Fig. 6c). At a CyA concentration
363 that did not affect wt cells (arrow in Fig. 6c), T cell activation of $CD28^{-/-}$ T cells was clearly
364 inhibited (Fig. 6c,d). Thus, compared to wt cells $CD28^{-/-}$ T cells are hypersensitive to CyA. In
365 contrast, $CD28^{-/-}$ T cells with forced miR-17~92 expression were normally activated (Fig. 6c,
366 d). In fact, at higher CyA concentrations the "rescue" T cells were even more resistant to CyA
367 inhibition than wt T cells (Fig. 6c). These findings were further corroborated by the analysis of
368 cell size which revealed that in the presence of low dose CyA the blasting defect of $CD28^{-/-}$ T
369 cells was compensated for by transgenic miR-17~92 (Fig. 6e). Finally, we assessed nuclear
370 translocation of activated NFATC2 as a direct readout of calcineurin activity. ImageStream
371 analysis of T cells activated in the presence of 6.25ng/ml CyA showed T cells with cytoplasmic

372 (top row) or nuclear (lower row) NFATC2 (Fig. 6f). Quantification of this data demonstrated
373 that the presence of a low CyA concentration reduced nuclear NFATC2 translocation in CD28^{-}
374 $^{/-}$ T cells but was restored in "rescue" cells (Fig. 6g). Thus, the miR-17~92 transgene replaced
375 CD28-enhanced calcineurin signals for blasting, CD69 upregulation and nuclear translocation
376 of NFATC2.
377
378 **miR-17~92 is necessary for repression of a subset of genes during T cell activation**
379 Finally, we examined whether miR-17~92 was physiologically required to shape the molecular
380 program triggered by CD28 engagement. We repeated transcriptome analysis with RNA-seq
381 on naïve and activated (24h) CD4^{+} T cells from T$^{1792\Delta/\Delta}$, wt and T$^{1792tg/tg}$ mice but added CD28^{-}
382 $^{/-}$ and "rescue" T cells. The correlation of miR-17~92 target gene expression levels with the
383 first RNA-seq experiment (Fig. 5) was very high (Suppl. Fig. 7a). A PCA showed that the
384 transcriptomes of naïve T cells of all 5 genotypes were closely related (Fig. 7a). However, after
385 T cell activation (PC1, 67.6% of variance) the 5 genotypes formed 5 distinct groups that were
386 separated on PC2 (5.6% of variance). Notably, the "rescue" samples were located between
387 CD28$^{-/-}$ and T$^{1792\Delta/\Delta}$, wt and T$^{1792tg/tg}$ T cells (Fig. 7a). This implies that transgenic miR-17~92
388 partially restored the genetic networks dysregulated by CD28-deficiency. Thus, the PCA
389 analysis supported the notion that the phenotypic rescue (Figs. 2-4) was a consequence of a
390 partially restored transcriptome rather than a transgene artifact. Moreover, compared to all
391 genes without a miR-17~92 seed match the miR-17~92 target gene set defined earlier (Suppl.
392 Table 1) was overall derepressed in CD28$^{-/-}$ T cells compared to wt cells (Fig. 7b and Suppl.
393 Fig. 7b). It is important to note that these cells have an untouched miR-17~92 locus and
394 therefore should repress miR-17~92 target genes like wt cells. However, the absence of CD28
395 resulted in increased expression of those genes. This result demonstrated that CD28-dependent
396 effects normally rely on miR-17~92 to repress dozens of genes during T cell activation.
397 Remarkably, expression of target genes was corrected in "rescue" cells (Fig. 7c and Suppl. Fig.
398 7b). Thus, transgenic miR-17~92 repressed the physiologic targets that were derepressed in
399 CD28$^{-/-}$ T cells.
400 However, the molecular rescue effect on the entire transcriptome was incomplete (Fig. 7a). In
401 order to determine which transcripts were restored and whether they were regulated
402 transcriptionally or posttranscriptionally, we performed unsupervised hierarchical clustering of
403 the same genes as shown in Fig. 5b but used the gene expression values from the 2nd dataset
404 with all 5 genotypes. At 24h, one gene cluster stood out in which "rescue" T cells were more
405 similar to wt and T$^{1792tg/tg}$ cells than CD28$^{-/-}$ and T$^{1792\Delta/\Delta}$ cells (Fig. 7d, box). Genes in this cluster
406 contained several NFAT-dependent transcripts including *IL-4, IL-12a, IL12rb2, IL-21* and
407 *IFNγ* (Suppl. Table II, Fig. 6b). Importantly, *Cd44, IL-21, Tbx-21 and IFNγ* transcripts, also

408 contained in this cluster, were reduced in CD28$^{-/-}$ compared to wt cells (Fig. 7e). In contrast,
409 transgenic miR-17∼92 partially or completely restored these transcripts in "rescue" cells to wt
410 levels. Furthermore, T$^{1792tg/tg}$ T cells expressed supraphysiologic mRNA levels (Fig. 7e). Thus,
411 the phenotypic rescue of CD44 and IFNγ in CD28$^{-/-}$ T cells (Fig. 2-4) can at least partially be
412 attributed to increased expression of these genes driven by the miR-17∼92 transgene in
413 "rescue" cells.
414 Conversely, as illustrated above (Fig. 7b) many direct targets were not only derepressed in
415 T$^{1792\Delta/\Delta}$ but also in CD28$^{-/-}$ cells. Several genes (e.g. *Rcan3, Nrbp1, Rnf38 and Rnf167*) were
416 similarly derepressed in CD28$^{-/-}$ and T$^{1792\Delta/\Delta}$ cells and expression was restored in "rescue" cells
417 to levels similar to wt and even further repressed in T$^{1792tg/tg}$ cells (Fig. 7f). Others, such as
418 *Phlpp2* and *Cyld* were clearly regulated by miR-17∼92 but expression differed in CD28$^{-/-}$ and
419 T$^{1792\Delta/\Delta}$ cells (Fig. 7f). For one of these targets, *Rcan3*, we confirmed this expression pattern
420 using targeted proteomics for absolute quantification (Fig. 7g). This suggests that these targets
421 are sensitive to regulation by miR-17∼92 and their derepression in CD28$^{-/-}$ T cells is largely
422 attributed to reduced repression by miR-17∼92. Collectively, the data demonstrates that miR-
423 17∼92 is necessary for CD28-induced gene repression.

424 **Discussion**

425 T cell activation depends on TCR and CD28 engagement to trigger complex molecular
426 mechanisms including activation of the PI3K, NF-κB and calcineurin/NFAT pathways. Intense
427 research in the past decades uncovered many molecules that transmit TCR and CD28 signals [2].
428 Most studies focused on proteins as signaling intermediates but we and others previously
429 reported that combined engagement of TCR and CD28 also alters expression of non-coding
430 RNAs. Most miRNAs are downregulated after T cell activation but a few, including miR-
431 17~92, remain relatively constant or are slightly induced [20,40]. This suggests that miR-17~92
432 might be functionally relevant during T cell activation. We previously found that miR-17~92
433 was induced after combined stimulation of TCR and CD28 in vitro but not after TCR
434 stimulation alone [20]. These findings were confirmed and extended to the natural ligands
435 CD80/CD86. Heterozygosity or absence of CD80/CD86 on B cells resulted in a dose-dependent
436 reduction in miR-17 induction in co-cultured T cells while deficiency or blockade of CTLA-4
437 resulted in increased miR-17 expression [41]. Furthermore, stimulating T cells with antibodies
438 directed to CD3 is sufficient to induce proliferation in $T^{1792tg/tg}$ T cells [21]. Collectively, these
439 studies suggest that T cell activation, CD28 and miR-17~92 are intimately linked. However,
440 their relation is poorly understood. Here, we tested whether transgenic miR-17~92 was
441 sufficient to substitute for the absence of CD28 and whether miR-17~92 was required for
442 CD28-mediated T cell activation. We found an unexpectedly potent rescue effect both in vitro
443 and in vivo. Many defects of $CD28^{-/-}$ T cells were functionally compensated for by the miR-
444 17~92 transgene. This is notable for two reasons. First, miR-17~92 is a non-coding RNA and
445 second, miRNAs are negative regulators. Thus, overexpression of an inhibitory RNA was
446 sufficient to enable T cell activation in the absence of CD28. However, the miR-17~92
447 transgene did not equally restore all investigated parameters. For instance, the transcriptome
448 was incompletely restored while i.c. IL-2 and the relative number of $CD44^{+}$ cells were even
449 higher in $T^{1792tg/tg}$ than "rescue" T cells. Moreover, although *Phlpp2* was clearly regulated by
450 miR-17~92, it was not derepressed in $CD28^{-/-}$ T cells. Thus, CD28 must control pathways that
451 are independent of miR-17~92 and not all molecular programs are equally sensitive to miR-
452 17~92 regulation. Nevertheless, we observed a graded rescue of some parameters with a single
453 or two copies of the miR-17~92 transgene. This data is consistent with recent findings that
454 sensing of costimulatory ligands in vivo is analog, not digital. Commitment to T_{FH}
455 differentiation appears to require a higher level of CD28 engagement than commitment to
456 proliferation or CD62L downregulation [41]. The tight connection between CD28 and miR-
457 17~92 [REFS 20,41] together with the data described here might explain why T_{FH} are particularly
458 sensitive to miR-17~92 [22,23] and opens the possibility that miRNAs of the miR-17~92 cluster
459 could be leveraged to tune T cell activation/costimulation.

460 To analyze the molecular mechanism by which miR-17~92 enabled T cell activation
461 in the absence of CD28 we took advantage of a multi-layer approach. RNA-Seq analysis of T
462 cells with miR-17~92 loss- or gain of function and sampled over a time course revealed that
463 miR-17~92 mainly influenced the transcriptome after T cell activation, a finding consistent
464 with phenotypic analysis of ex vivo characterized naïve T cells. There is an emerging notion
465 that evidence of miRNA binding combined with differential gene expression in primary cells
466 constitutes a precise approach to empirically define miRNA:target relationships [16,33]. We
467 refined this approach by combining EISA with AHC to discriminate whether differentially
468 expressed gene clusters were primarily regulated transcriptionally or posttranscriptionally. This
469 analysis provides a highly granular view of miRNA-mediated gene regulation. Specifically,
470 pathway and regulon enrichment analysis revealed that miR-17~92 enhanced the
471 calcineurin/NFAT pathway. Consistent with this, a gene cluster enriched for genes that
472 positively correlated with miR-17~92 was mainly transcriptionally regulated and contained
473 many genes known to be regulated by NFAT TF including genes for various $CD4^+$ T cell
474 subsets such as T_{FH} (*IL-21*) and T_H1 (*Tbx-21 and IFNγ*). Experiments with pharmacologic CNIs
475 confirmed that miR-17~92 functionally promoted the calcineurin/NFAT pathway. Importantly,
476 transgenic miR-17~92 partially restored the molecular program that was defective in $CD28^{-/-}$
477 T cells. In particular, expression of key NFAT-regulated genes found to be driven by miR-
478 17~92 in CD28-sufficient T cells were restored by the transgene in CD28-deficient T cells.
479 Although CD28 is critical for early T cell priming, CD28 costimulation continues to be
480 important for days [4]. Our data shows that in the first 24h miR-17~92 has important functions
481 by promoting T cell activation and expression of TF, cytokines and cytokine receptors required
482 for differentiation into multiple T cell subsets. We and others previously demonstrated that
483 miR-17~92 also supports T cell differentiation and/or subset specific functions at later time
484 points, e.g. by repressing lineage inappropriate TF and facilitating PI3K signaling [22,23]. We
485 propose that miR-17~92 acts as a downstream mediator or amplifier of the molecular program
486 triggered by combined TCR/CD28 engagement. However, how CD28/T cell activation is
487 linked molecularly to miR-17~92 expression remains poorly understood. Although the
488 presence of myc binding sites is suggestive for transcriptional regulation [42], miRNA biogenesis
489 can be controlled by extracellular cues [43] and in embryonic stem cells maturation of miR-17~92
490 into mature miRNAs is also regulated posttranscriptionally [44]. Future studies are needed to
491 unravel how CD28 costimulation/T cell activation regulate miR-17~92 expression.
492 Nevertheless, our data demonstrates that miR-17~92, induced by the combined triggering of
493 TCR and CD28, is required to mediate gene repression that indirectly promotes gene
494 expression. Thus, miR-17~92 is part of a feed forward loop.

How can a microRNA cluster that negatively regulates genes promote gene expression and bypass the requirement for CD28 costimulation? To shed light on this question we first defined miR-17~92 target genes in T cells using miR-17~92 gain- and loss of function as well as AHC. Next we demonstrated that these same genes were elevated in stimulated CD28$^{-/-}$ T cells. We conclude that during T cell activation miR-17~92 is required to repress this set of genes. Previous work demonstrated that miR-17~92 promotes the PI3K, NF-κB and mTOR pathways. Here we demonstrate that it also enhances the calcineurin/NFAT pathway. We noticed that the identified, empirically validated miR-17~92 target gene network contains multiple negative regulators of the PI3K (*Phlpp2*), NF-κB (*Cyld*) and NFAT (*Cyld, Rcan3*) pathways. Furthermore, the list contains poorly characterized known or suspected tumor suppressors, genes related to cell growth, proliferation, migration and cancer (e.g. *Nkiras1, Nrbp1, Tgif1, Ugp2, Wdr26, Zbtb4*) as well as known or suspected E3 ligases (*Ankib1, Dcaf8, Rnf38* and *Rnf167*). Since miR-17~92 promotes proliferation and can be oncogenic it is suggestive that repression of at least some of these genes contributes to proliferation after T cell activation.

The importance of removing negative regulators to enable T cell activation is illustrated by limited experimental evidence that gene deletion can partially rescue CD28-deficiency. For instance, genetic deletion of Casitas B lymphoma-b protein (*Cbl-b*) is sufficient to restore IL-2 production and proliferation in CD28$^{-/-}$ T cells. However, neither IFNγ, IL-4 or ICOS expression nor GC formation were restored [45,46]. Thus, while loss of Cbl-b uncoupled T cells from the strict requirement for CD28 costimulation, it could not restore all aspects of CD28-mediated costimulation. Similarly, genetic ablation of PTEN or TRAF6 restored proliferation and IL-2 production in CD28$^{-/-}$ CD4^{+} T cells [47,48]. In addition, peripheral Cyld$^{-/-}$ T cells display increased proliferation, IFNγ and IL-2 production upon activation. Thus, Cyld-deficient T cells are hyperresponsive to stimulation and therefore Cyld is another important restrainer of T cell activation [35]. Because of these genetic examples it was noted before that the default consequence of TCR triggering is preventing T cell activation and induction of anergy [49]. As a group of genes, negative regulators impose a requirement for a costimulatory signal to actively remove these brakes to allow a productive T cell response. CD28 costimulation therefore serves a dual purpose by enhancing TCR signaling and simultaneously overcoming T cell repression [12,48,49]. Interestingly, *Cbl-b, PTEN* and *Cyld* are all directly targeted by miR-17~92. Importantly, during T cell activation the inhibitors are not completely eliminated as is the case in the genetic deletion systems. Rather, TRAF6, PTEN and Rcan3 expression decreases but these genes remain expressed at substantial levels and Cbl-b expression even increases (induced by NFAT) [47]. Thus, although experimental deletion can demonstrate that a given gene has the potential to act as a powerful negative regulator, its physiologic function is more delicate to uncover and complete deletion likely overestimates the contribution of the gene under

531 investigation. To date no single gene or pathway can explain the function of CD28
532 costimulation. More likely, multiple negative regulators need to be removed and multiple
533 pathways need to be induced. Our results illustrate that miR-17~92 can exert complex
534 regulation of the T cell transcriptome through direct and indirect gene regulation. Mammalian
535 gene expression is rarely digital and controlled by multiple layers of molecular mechanisms.
536 By combining transcriptional with posttranscriptional gene regulation, animals can achieve
537 complex gene expression with relatively simple promoters [14]. It is conceivable that precise
538 control of genetic programs is particularly important for an exponential process like clonal T
539 cell expansion. Even minor changes in setting the T cell activation threshold or the rate of
540 proliferation or survival could result in major consequences for the host organism. Since
541 miRNAs are important sculptors of the transcriptome they are ideally suited to mediate
542 controlled release from multiple restraining proteins preventing T cell activation [14]. Therefore,
543 genes like *Rcan3, Nrbp1, Rnf38* and *Rnf167* are of particular interest for further investigation
544 since they are equally derepressed in $CD28^{-/-}$ and $T^{1792\Delta/\Delta}$ $CD4^{+}$ T cells but very sensitive to
545 regulation by miR-17~92 since their expression in "rescue" cells is similar to wt cells. It will
546 be interesting to determine if their repression contributes to bypassing CD28 in "rescue" T cells.
547 Other miR-17~92-regulated genes such as *Cyld* are also of interest but miR-17~92-
548 independent mechanisms must be operational since its expression is not affected as much in
549 $T^{1792\Delta/\Delta}$ as in $CD28^{-/-}$ $CD4^{+}$ T cells. Clearly, additional studies are needed to decipher the relative
550 contributions of each individual or combinations of target genes in primary T cells and
551 oncogenesis because miRNA regulation is highly cell type and context dependent [16].
552 Nevertheless, our findings greatly expand the list of high confidence miR-17~92 targets with
553 a suspected function in T cells.
554 In summary, we propose a model in which miR-17~92 constitutes an important mediator of T
555 cell activation/CD28 costimulation by serving as a gatekeeper of a network of restrainers
556 controlling at least 3 central pathways for T cell activation and function. In this model, non-
557 coding RNA-mediated repression of inhibitors supports transcriptional induction of genes
558 necessary for further T cell differentiation and function (e.g. CD44, IL-21, Tbx21, IFNγ).
559 Importantly, we not only show that transgenic miR-17~92 is largely sufficient to substitute for
560 CD28-deficiency but that miR-17~92 is physiologically required to shape the transcriptome
561 after CD28 costimulation and that miR-17~92 overexpression in CD28-sufficient T cells
562 results in "super-costimulation". In support of the proposed model, constitutive transgenic miR-
563 17~92 expression leads to a lupus-like systemic autoimmune syndrome [21], not unlike the ones
564 observed in mice deficient in *Cbl-b, PTEN, TRAF6* or *Cyld* [35,45,46,50,51]. Our results support the
565 consideration of miR-17~92 or its target genes for pharmacologic intervention or for its
566 integration into engineered cellular therapies.

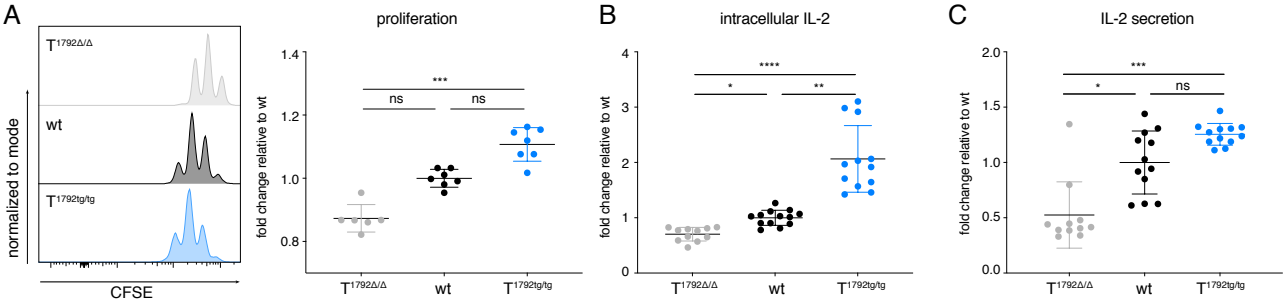

Figure 1. miR-17~92 regulates T cell proliferation and Interleukin-2 production
A) Proliferation of CFSE labelled T1792Δ/Δ (grey), wt (black) and T1792tg/tg (light blue) CD4+ T cells activated for 48h with plate-bound αCD3/αCD28 mAbs. B) Quantification of flow cytometric intracellular IL-2 staining in CD4+ cells stimulated for 3h with PMA/Iono/BFA. C) IL-2 secretion measured by ELISA in culture supernatants at 48h. Error bars show mean ±SD, Dunn's multiple comparison test, p values: ns=not significant, *<0.05 **<0.002 ***<0.0002 ****<0.0001. Data represent 2-3 independent experiments with 3-4 biological replicates per group.

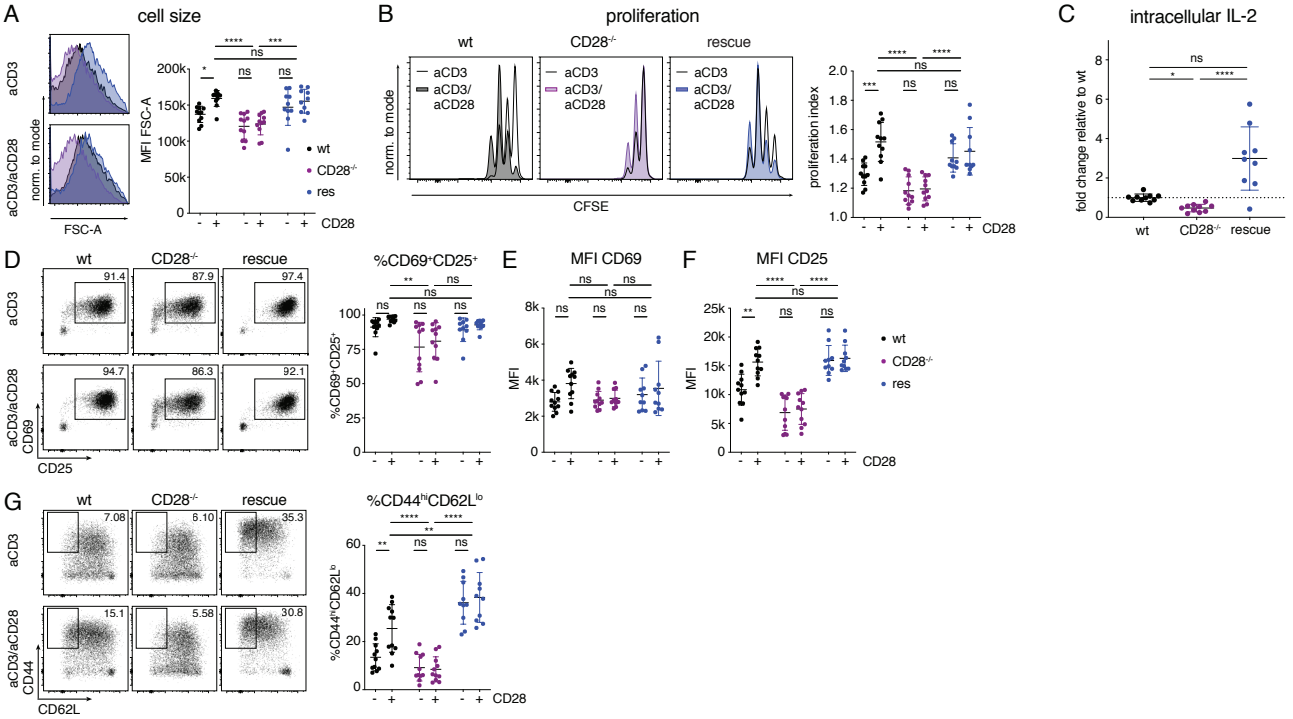

Figure 2. Transgenic miR-17~92 enables T cell activation of CD28-deficient T cells in vitro.
wt (black), CD28-/- (purple), rescue (dark blue). A) Blasting of CD4+ T cells shown as MFI of FSC-A of the lymphocyte gate. B) Proliferation measured by CFSE dilution, gated on viable CD4+ T cells. Representative histograms of each genotype activated without (blank) or with (colored) αCD28. C) Quantification of flow cytometric intracellular IL-2 staining in CD4+ cells stimulated for 3h with PMA/Iono/BFA. D-G) CD4+ T cells were stimulated for 48h with plate-bound αCD3 with (+) or without (-) αCD28 and investigated for expression of early activation markers CD25/CD69 expression (D, E, F) as well as CD44/CD62L expression (G). Data from 3 independent experiments with 3-4 biological replicates per group. Error bars represent mean ±SD, Tukey's or Hom-Sidak's multiple comparison test; p values: ns=not significant, *<0.05 **<0.002 ***<0.0002 ****<0.0001

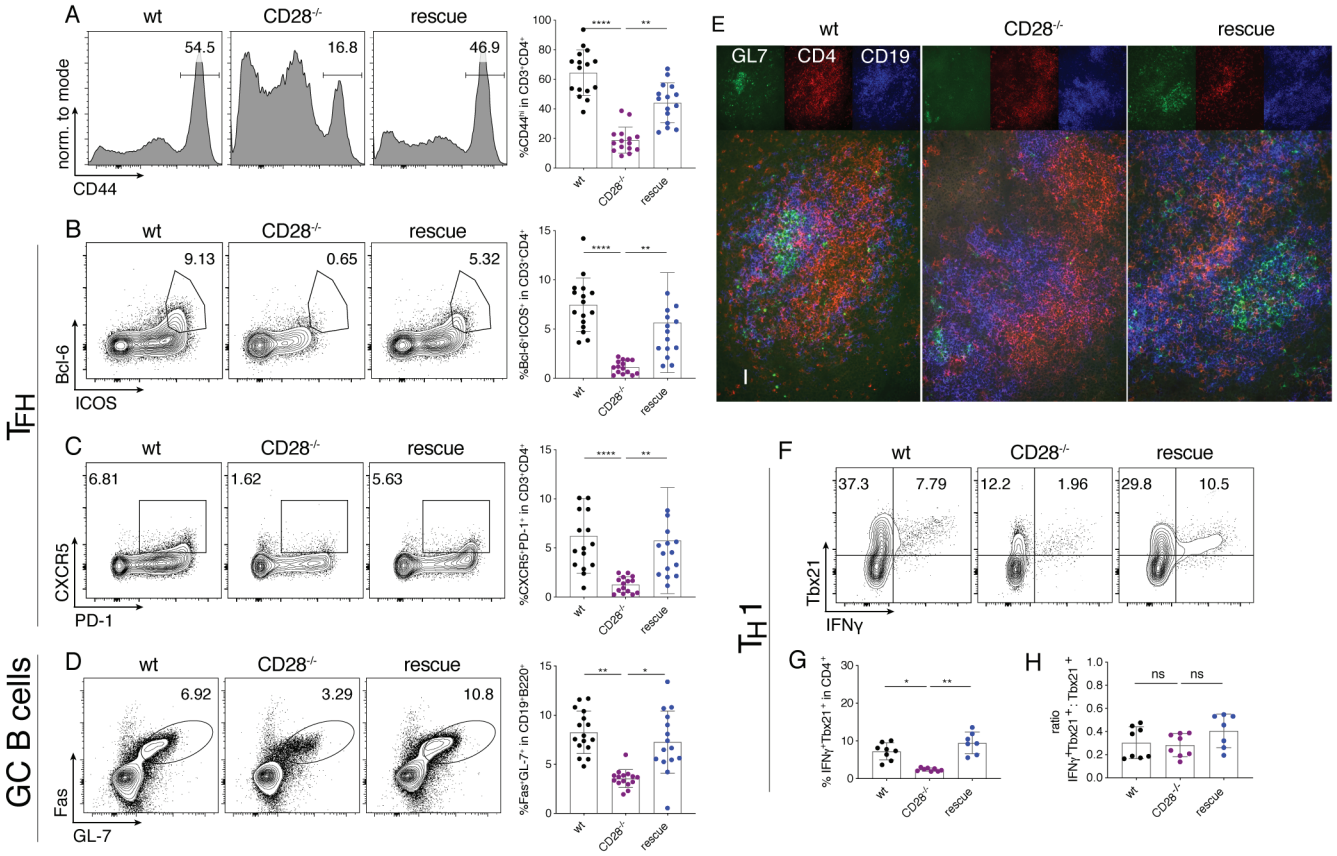

Figure 3. Transgenic miR-17~92 enables T cell activation of CD28-deficient T cells in vivo.

6-8 week old mice were infected with LCMV Armstrong; spleens were analyzed at d8 post infection. wt (black), CD28-/- (purple), rescue (dark blue). A-D) represent data from 4 independent experiments with 4 mice per group, pre-gating on viable CD4+CD3+ or viable CD19+B220+ cells. A) CD44 expression. B) relative number of Bcl6+ICOS+ population (TFH) C) relative number of CXCR5+PD-1+ population (TFH) D) relative number of Fas+GL7+ population (GC B cells) E) Cryosections of spleens stained for GL-7 (green), CD4 (red) and CD19 (blue). Scale bar 40μm. Splenocytes were re-stimulated with GP-64 and BFA for 4h and investigated for TH1 phenotype, pre-gated on viable CD3+CD4+ cells. Shown are 3 independent experiments with 4 biological replicates per group. F) representative contour plots of Tbx21 and IFNγ expression G) Quantification of Tbx21+IFNγ+ CD3+CD4+ cells H) ratio of Tbx21+IFNγ+ to total Tbx21+ cells. Error bars represent mean with SD, Dunn's multiple comparison test; p values: ns=not significant, *<0.05, **<0.002, ***<0.0002, ****<0.0001

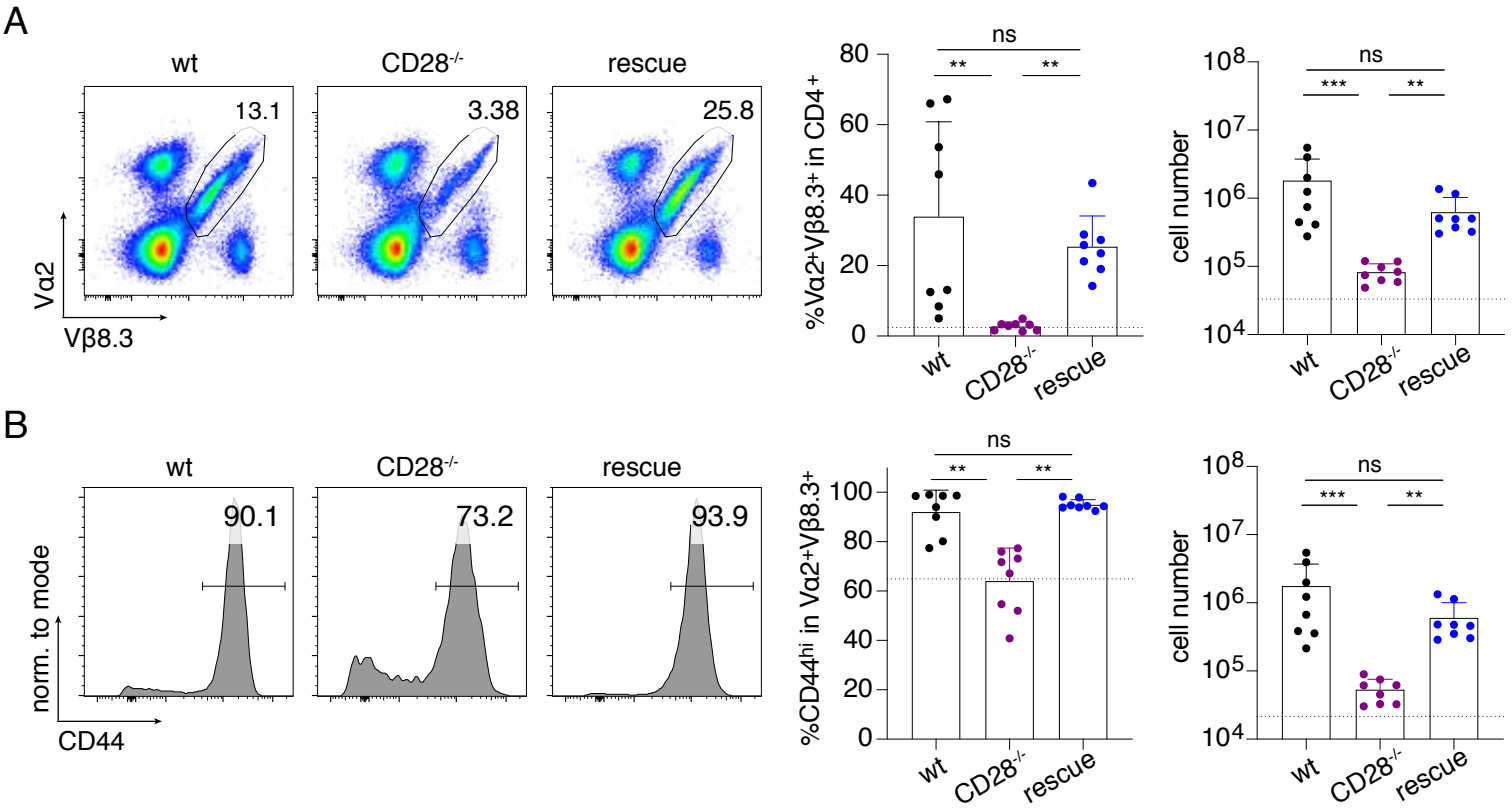

Figure 4. Restoration of T cell activation of CD28-deficient T cells by miR-17~92 is cell intrinsic.
Adoptive transfer of naïve SMARTA+ CD4+ T cells into CD28-/- hosts, subsequent LCMV Armstrong infection and analysis of organs at d8 post infection. Donor genotypes wt (black), CD28-/- (purple), rescue (dark blue). Dotted line indicates recipient's intrinsic Vα2+Vβ8.3+ population measured in a non-transferred control host. A) Vα2+Vβ8.3+ cells from peripheral LN pre-gated on viable, CD3+CD4+ cells B) CD44 expression in Vα2+Vβ8.3+ population from peripheral LN. 2 independent experiments, 4 recipients per group. Error bars represent mean ±SD, Dunn's multiple comparison test, p values: ns=not significant, *<0.05, **<0.002, ***<0.0002. See also Figure S1 for spleen and mesenteric LN.

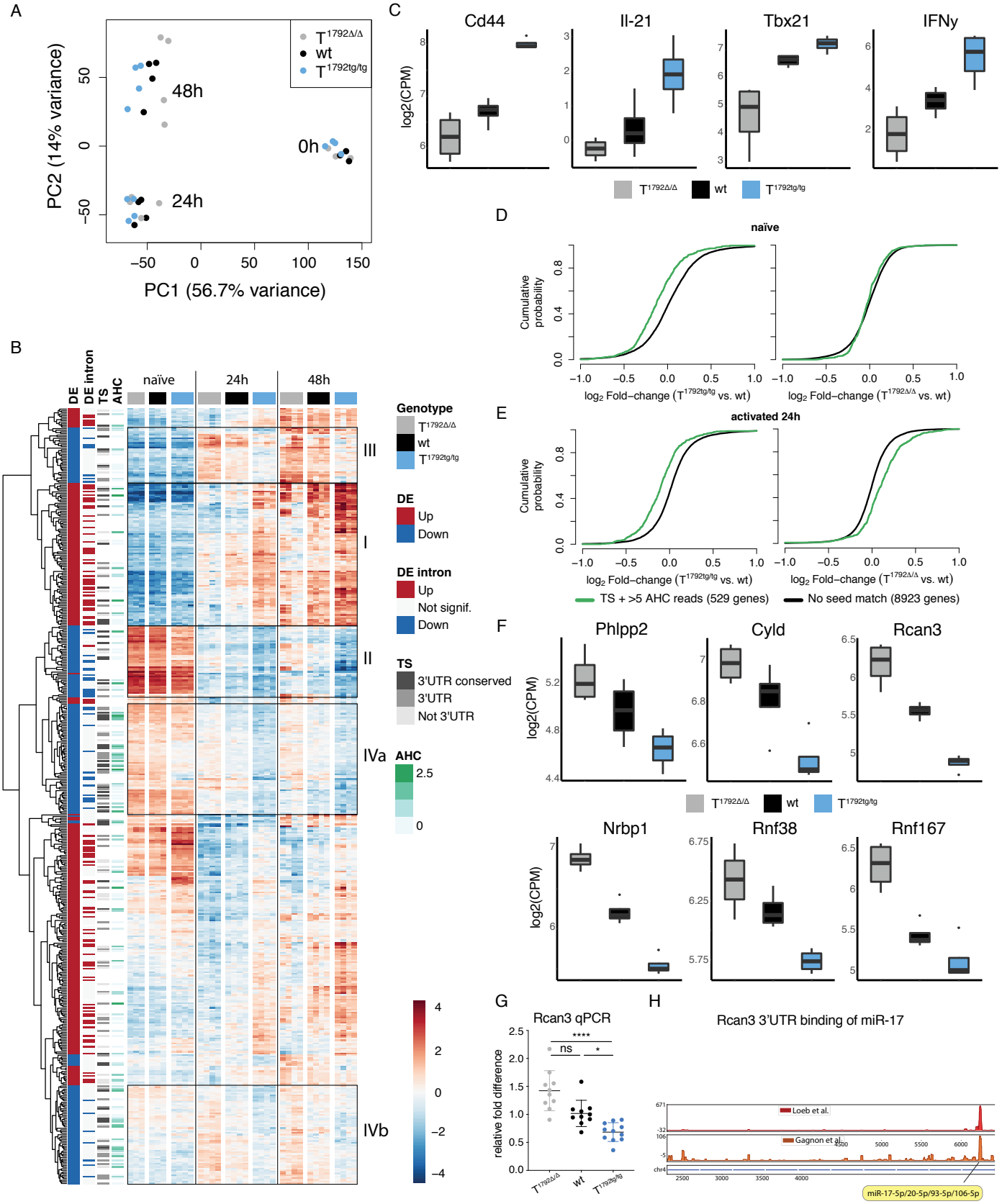

Figure 5. miR-17~92 shapes the transcriptome after T cell activation.
Naïve CD4+ T cells from T1792Δ/Δ (grey), wt (black) and T1792tg/tg (light blue) were activated with plate-bound αCD28 and αCD3 for 0, 24h and 48h. Total RNA was extracted for bulk RNA sequencing. A) PCA (PC1 vs. PC2) based on the 25% most variable genes. B) Hierarchical clustering of the set of genes selected with abs(log2FC)>1 & adj.P.Val<0.001 in the T1792tg/tg vs. T1792Δ/Δ comparison at 24h. The heatmap displays the centered log of counts per million, with blue indicating low and red indicating high expression. Annotations: "DE" indicates the fold change direction, "DE intron" indicates if significant changes are observed in EISA analysis, "TS" indicates presence (grey) or absence (blank) of a seed match and its location and "AHC" indicates the 3'UTR signal intensity in HITS-CLIP data. Boxes I-IVb designate gene clusters. C) Examples of genes in cluster I. D, E) Genome-wide transcriptome analysis, presented as the log2 value of the gene-expression ratio for each gene versus the cumulative fraction of all log2 ratios in naïve (D) and 24h activated (E). Shown is the miR-17 seed family for T1792tg/tg vs. wt and T1792Δ/Δ vs. wt comparisons. Black curve: all genes without a seed match and ≤5 AHC reads; green: subset of genes with a seed sequence for the seed family and >5 reads in the AHC. F) Examples of genes defined as empirically validated miR-17~92 targets. log2 RNA expression level in activated CD4+ T cells, numbers correspond to FDR<0.05. G) Rcan3 mRNA expression detected by qPCR 24h after activation; shown are pooled data from three independent experiments, normalized to wt. T1792Δ/Δ (grey), wt (black), T1792tg/tg (light blue). mRNA expression normalized to 18S rRNA. Values are means ±SD, Dunn's multiple comparison test, p values: ns=not significant, *<0.05 ****<0.0001. H) Binding sites of Argonaute 2 in 3'UTR of Rcan3 detected by HITS-CLIP; predicted miR17 binding site indicated by yellow flag. See also Figure S3 and Suppl. Table S1.

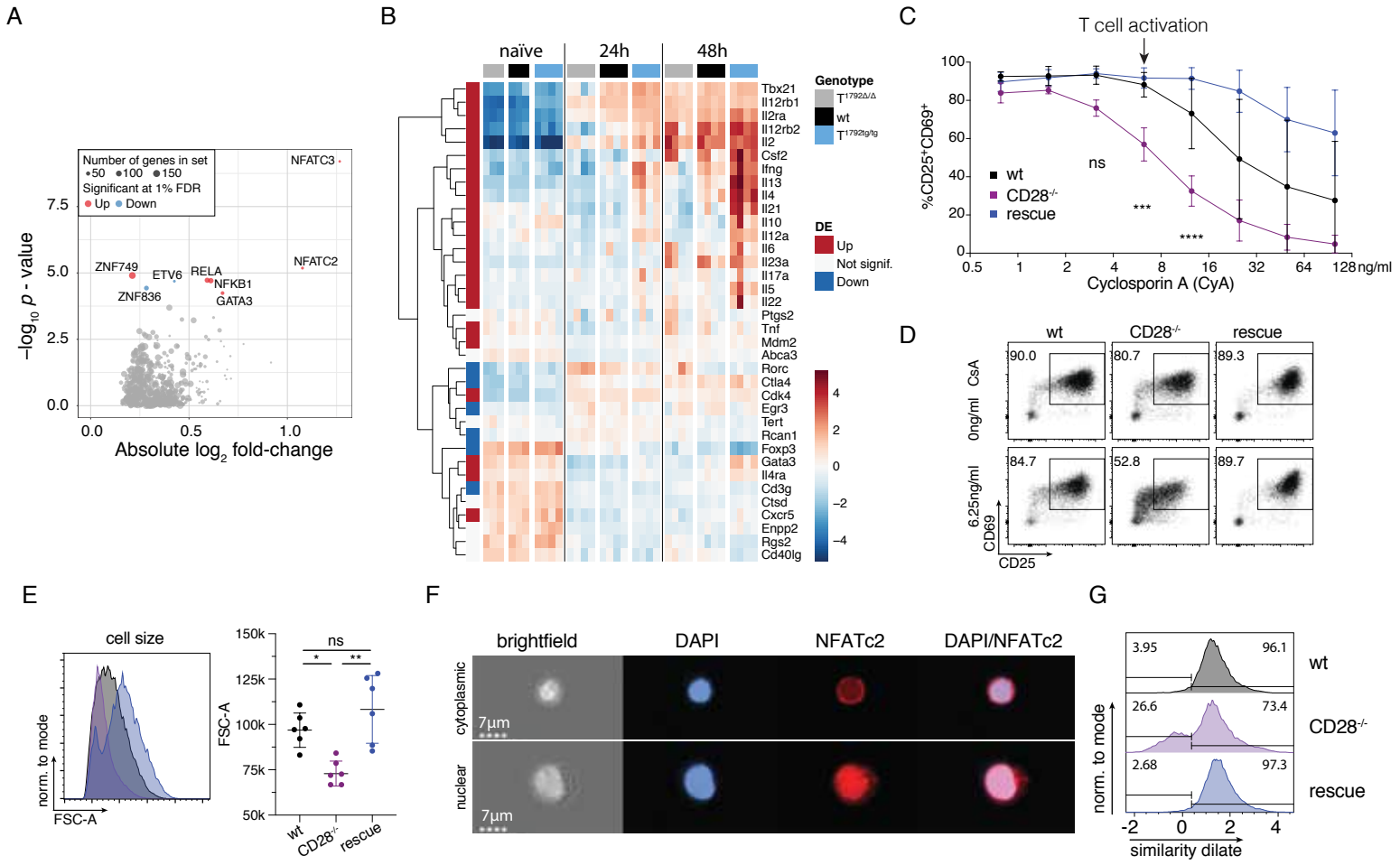

Figure 6. miR-17~92 promotes the calcineurin/NFAT pathway in CD4+ T cells

A, B) Dataset from Figure 5. Naïve CD4+ T cells from T1792Δ/Δ (grey), wt (black) and T1792tg/tg (light blue) were activated with plate-bound αCD28 and αCD3 for 0, 24h and 48h. Total RNA was extracted for bulk RNA sequencing.

A) Volcano plot showing the absolute log2 fold change and -log10 p value from regulon analysis. A threshold of 1% FDR was applied. Dot size indicates number of genes within each regulon and colors indicate fold change direction. B) Heatmap of genes under NFATC2_D and NFATC3_D regulons plus several known activated genes in CD4+ T cells (Il10, Il12a, Il6, Rorc, Il23a). Hierarchical clustering was applied on genes. Centered log of counts per million is displayed, with blue indicating low and red indicating high expression. C) CD4+ wt (black), CD28-/- (purple) and rescue (dark blue) cells were activated for 48h in the presence of increasing concentrations of cyclosporin A (CyA) as indicated and stained for CD25 and CD69. Shown are 2 independent experiments, error bars represent means ±SD. Tukey's multiple comparison, p values: **<0.002, ****<0.0001 refer to the difference between CD28-/- and wt. D) representative FACS plots of CD25/CD69 expression in viable CD4+ T cells activated for 48h with no or 6.25ng/ml CyA. E) influence of 6.25ng/ml CyA on blasting (FSC-A of the lymphocyte gate) of viable CD4+ cells. F) Imagestream analysis of CD4+ T cells, activated for 48h in presence of 6.25ng/ml CyA; DAPI (blue) and NFATc2 (red) staining. Examples for cytoplasmic (top) and nuclear (bottom) NFATc2 in a CD28-/- sample. G) histograms of the similarity dilate indicative of the co-localization of NFATc2 and DAPI signals; gates indicate the nuclear (high similarity dilate) and the cytoplasmic population (low similarity dilate). See also Figures S4 – S6.

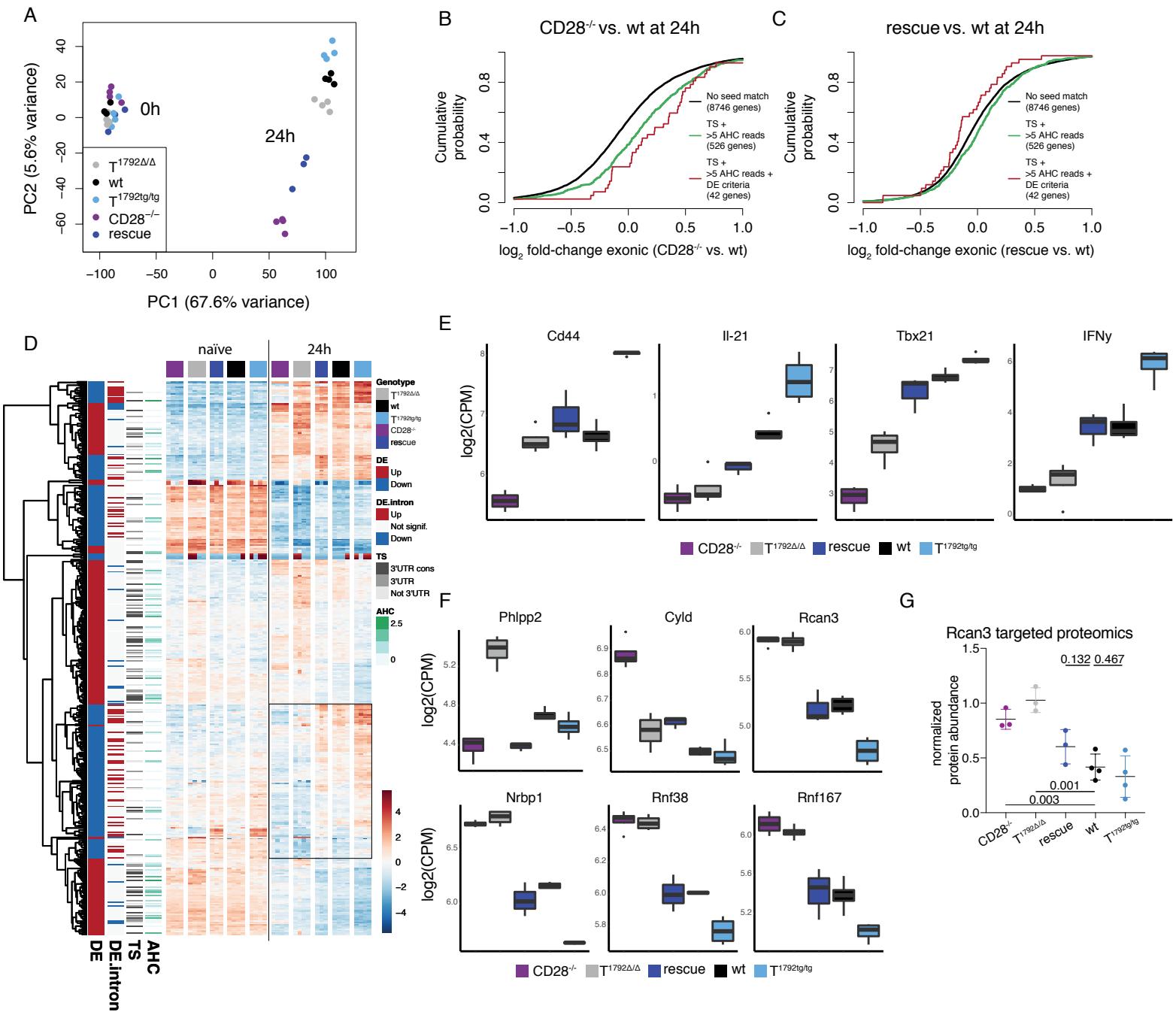

Figure 7. miR-17~92 is necessary for repression of a subset of genes during T cell activation
CD4+ T cells from T1792Δ/Δ (grey), wt (black), T1792tg/tg (light blue), CD28-/- (purple) and rescue (dark blue) mice were activated for 24h. Total RNA was extracted for sequencing. A) PCA (PC1 vs. PC2) based on the 25% most variable genes. B) Genome-wide transcriptome analysis, presented as the log2 value of the gene-expression ratio for each gene versus the cumulative fraction of all log2 ratios. Shown are the contrasts between activated samples separated by the miR-17 seed family for the comparison CD28-/- vs. wt (B) and rescue vs. wt (C). Black curve: genes without a seed match, ≤5 AHC reads, and no differential expression in the second RNA sequencing. Green: genes with a conserved binding site for the miR-17 seed family (TS) and >5 reads in the AHC, red: genes with a conserved binding site for the miR-17 seed family (TS), >5 reads in the AHC and differential expression in the second RNA sequencing data set. D) Hierarchical clustering of the set of genes selected with abs(log2FC)>1 & adj.P.Val<0.001 in the T1792tg/tg vs. T1792Δ/Δ comparison at 24h. The heatmap displays the centered log of counts per million, with blue indicating low and red indicating high expression. E) Examples of transcripts that were restored in "rescue" compared to CD28-/- T cells, i.e. contained in the box of Fig. 7d. F) Examples of direct miR-17~92 targets. E, F: log2 mRNA expression in activated CD4+ T cells; numbers correspond to FDR<0.05. G) Rcan3 protein abundance measured by targeted proteomics 24h after activation. CD28-/- (purple), T1792Δ/Δ (grey), rescue (dark blue), and T1792tg/tg (light blue) are compared to wt (black). Proteins were isolated from the same cells for targeted proteomics of Rcan3 and total RNA sequencing. Numbers indicate p values from t-test. See also Figure S7.

567 **Figure legends**

568 **Figure 1**

569 **miR-17~92 regulates T cell proliferation and Interleukin-2 production**

570 A) Proliferation of CFSE labelled $T^{1792\Delta/\Delta}$ (grey), wt (black) and $T^{1792tg/tg}$ (light blue) $CD4^+$ T
571 cells activated for 48h with plate-bound αCD3/αCD28 mAbs. B) Quantification of flow
572 cytometric intracellular IL-2 staining in $CD4^+$ cells stimulated for 3h with PMA/Iono/BFA.
573 C) IL-2 secretion measured by ELISA in culture supernatants at 48h. Error bars show mean
574 ±SD, Dunn's multiple comparison test, p values: ns=not significant, *<0.05 **<0.002
575 ***<0.0002 ****<0.0001. Data represent 2-3 independent experiments with 3-4 biological
576 replicates per group.
577

578 **Figure 2**
579 **Transgenic miR-17~92 enables T cell activation of CD28-deficient T cells in vitro**
580 wt (black), $CD28^{-/-}$ (purple), rescue (dark blue). A) Blasting of $CD4^+$ T cells shown as MFI of
581 FSC-A of the lymphocyte gate. B) Proliferation measured by CFSE dilution, gated on viable
582 $CD4^+$ T cells. Representative histograms of each genotype activated without (blank) or with
583 (colored) αCD28. C) Quantification of flow cytometric intracellular IL-2 staining in $CD4^+$
584 cells stimulated for 3h with PMA/Iono/BFA. D-G) $CD4^+$ T cells were stimulated for 48h with
585 plate-bound αCD3 with (+) or without (-) αCD28 and investigated for expression of early
586 activation markers CD25/CD69 expression (D, E, F) as well as CD44/CD62L expression (G).
587 Data from 3 independent experiments with 3-4 biological replicates per group. Error bars
588 represent mean ±SD, Tukey's or Hom-Sidak's multiple comparison test; p values: ns=not
589 significant, *<0.05 **<0.002 ***<0.0002 ****<0.0001
590

591 **Figure 3**
592 **Transgenic miR-17~92 enables T cell activation of CD28-deficient T cells in vivo**

593 6-8 week old mice were infected with LCMV Armstrong; spleens were analyzed at d8 post
594 infection. wt (black), $CD28^{-/-}$ (purple), rescue (dark blue). A-D) represent data from 4
595 independent experiments with 4 mice per group, pre-gating on viable $CD4^+CD3^+$ or viable
596 $CD19^+B220^+$ cells. A) CD44 expression. B) relative number of $Bcl6^+ICOS^+$ population (T_{FH})
597 C) relative number of $CXCR5^+PD\text{-}1^+$ population (T_{FH}) D) relative number of Fas^+GL7^+
598 population (GC B cells) E) Cryosections of spleens stained for GL-7 (green), CD4 (red) and
599 CD19 (blue). Scale bar 40µm. Splenocytes were re-stimulated with GP-64 and BFA for 4h
600 and investigated for T_H1 phenotype, pre-gated on viable $CD3^+CD4^+$ cells. Shown are 3
601 independent experiments with 4 biological replicates per group. F) representative contour
602 plots of Tbx21 and IFNγ expression G) Quantification of $Tbx21^+IFN\gamma^+$ $CD3^+CD4^+$ cells H)
603 ratio of $Tbx21^+IFN\gamma^+$ to total $Tbx21^+$ cells. Error bars represent mean with SD, Dunn's
604 multiple comparison test; p values: ns=not significant, *<0.05, **<0.002, ***<0.0002,
605 ****<0.0001
606

607 **Figure 4**
608 **Restoration of T cell activation of CD28-deficient T cells by miR-17~92 is cell intrinsic**

609 Adoptive transfer of naïve $SMARTA^+$ $CD4^+$ T cells into $CD28^{-/-}$ hosts, subsequent LCMV
610 Armstrong infection and analysis of organs at d8 post infection. Donor genotypes wt (black),
611 $CD28^{-/-}$ (purple), rescue (dark blue). Dotted line indicates recipient's intrinsic $V\alpha2^+V\beta8.3^+$
612 population measured in a non-transferred control host. A) $V\alpha2^+V\beta8.3^+$ cells from peripheral
613 LN pre-gated on viable, $CD3^+CD4^+$ cells B) CD44 expression in $V\alpha2^+V\beta8.3^+$ population
614 from peripheral LN. 2 independent experiments, 4 recipients per group. Error bars represent
615 mean ±SD, Dunn's multiple comparison test, p values: ns=not significant, *<0.05, **<0.002,
616 ***<0.0002. See also Figure S1 for spleen and mesenteric LN.

Figure 5
miR-17~92 shapes the transcriptome after CD4$^+$ T cell activation

Naïve CD4$^+$ T cells from T$^{1792\Delta/\Delta}$ (grey), wt (black) and T$^{1792tg/tg}$ (light blue) were activated with plate-bound αCD28 and αCD3 for 0, 24h and 48h. Total RNA was extracted for bulk RNA sequencing. A) PCA (PC1 vs. PC2) based on the 25% most variable genes. B) Hierarchical clustering of the set of genes selected with abs(log2FC)>1 & adj.P.Val<0.001 in the T$^{1792tg/tg}$ vs. T$^{1792\Delta/\Delta}$ comparison at 24h. The heatmap displays the centered log of counts per million, with blue indicating low and red indicating high expression. Annotations: "DE" indicates the fold change direction, "DE intron" indicates if significant changes are observed in EISA analysis, "TS" indicates presence (grey) or absence (blank) of a seed match and its location and "AHC" indicates the 3'UTR signal intensity in HITS-CLIP data. Boxes I-IVb designate gene clusters. C) Examples of genes in cluster I. D, E) Genome-wide transcriptome analysis, presented as the log2 value of the gene-expression ratio for each gene versus the cumulative fraction of all log2 ratios in naïve (D) and 24h activated (E). Shown is the miR-17 seed family for T$^{1792tg/tg}$ vs. wt and T$^{1792\Delta/\Delta}$ vs. wt comparisons. Black curve: all genes without a seed match and ≤5 AHC reads; green: subset of genes with a seed sequence for the seed family and >5 reads in the AHC. F) Examples of genes defined as empirically validated miR-17~92 targets. log2 RNA expression level in activated CD4$^+$ T cells, numbers correspond to FDR<0.05. G) Rcan3 mRNA expression detected by qPCR 24h after activation; shown are pooled data from three independent experiments, normalized to wt. T$^{1792\Delta/\Delta}$ (grey), wt (black), T$^{1792tg/tg}$ (light blue). mRNA expression normalized to 18S rRNA. Values are means ±SD, Dunn's multiple comparison test, p values: ns=not significant, *<0.05 ****<0.0001. H) Binding sites of Argonaute 2 in 3'UTR of Rcan3 detected by HITS-CLIP; predicted miR17 binding site indicated by yellow flag. See also Figure S3 and Suppl. Table S1.

Figure 6
miR-17~92 promotes the calcineurin/NFAT pathway in CD4$^+$ T cells

A, B) Dataset from Figure 5. Naïve CD4$^+$ T cells from T$^{1792\Delta/\Delta}$ (grey), wt (black) and T$^{1792tg/tg}$ (light blue) were activated with plate-bound αCD28 and αCD3 for 0, 24h and 48h. Total RNA was extracted for bulk RNA sequencing.
A) Volcano plot showing the absolute log2 fold change and -log10 p value from regulon analysis. A threshold of 1% FDR was applied. Dot size indicates number of genes within each regulon and colors indicate fold change direction. B) Heatmap of genes under NFATC2_D and NFATC3_D regulons plus several known activated genes in CD4$^+$ T cells (Il10, Il12a, Il6, Rorc, Il23a). Hierarchical clustering was applied on genes. Centered log of counts per million is displayed, with blue indicating low and red indicating high expression.
C) CD4$^+$ wt (black), CD28$^{-/-}$ (purple) and rescue (dark blue) cells were activated for 48h in the presence of increasing concentrations of cyclosporin A (CyA) as indicated and stained for CD25 and CD69. Shown are 2 independent experiments, error bars represent means ±SD. Tukey's multiple comparison, p values: **<0.002, ****<0.0001 refer to the difference between CD28$^{-/-}$ and wt. D) representative FACS plots of CD25/CD69 expression in viable CD4$^+$ T cells activated for 48h with no or 6.25ng/ml CyA. E) influence of 6.25ng/ml CyA on blasting (FSC-A of the lymphocyte gate) of viable CD4$^+$ cells. F) Imagestream analysis of CD4$^+$ T cells, activated for 48h in presence of 6.25ng/ml CyA; DAPI (blue) and NFATc2 (red) staining. Examples for cytoplasmic (top) and nuclear (bottom) NFATc2 in a CD28$^{-/-}$ sample. G) histograms of the similarity dilate indicative of the co-localization of NFATc2 and DAPI signals; gates indicate the nuclear (high similarity dilate) and the cytoplasmic population (low similarity dilate). See also Figures S4 – S6.

670 **Figure 7**
671 **miR-17~92 is necessary for repression of a subset of genes during T cell activation**
672 $CD4^+$ T cells from $T^{1792\Delta/\Delta}$ (grey), wt (black), $T^{1792tg/tg}$ (light blue), $CD28^{-/-}$ (purple) and rescue
673 (dark blue) mice were activated for 24h. Total RNA was extracted for sequencing. A) PCA
674 (PC1 vs. PC2) based on the 25% most variable genes. B) Genome-wide transcriptome
675 analysis, presented as the log2 value of the gene-expression ratio for each gene versus the
676 cumulative fraction of all log2 ratios. Shown are the contrasts between activated samples
677 separated by the miR-17 seed family for the comparison $CD28^{-/-}$ vs. wt (B) and rescue vs. wt
678 (C). Black curve: genes without a seed match, ≤5 AHC reads, and no differential expression
679 in the second RNA sequencing. Green: genes with a conserved binding site for the miR-17
680 seed family (TS) and >5 reads in the AHC, red: genes with a conserved binding site for the
681 miR-17 seed family (TS), >5 reads in the AHC and differential expression in the second RNA
682 sequencing data set. D) Hierarchical clustering of the set of genes selected with
683 abs(log2FC)>1 & adj.P.Val<0.001 in the $T^{1792tg/tg}$ vs. $T^{1792\Delta/\Delta}$ comparison at 24h. The heatmap
684 displays the centered log of counts per million, with blue indicating low and red indicating
685 high expression. E) Examples of transcripts that were restored in "rescue" compared to $CD28^-$
686 $^{/-}$ T cells, i.e. contained in the box of Fig. 7d. F) Examples of direct miR-17~92 targets. E, F:
687 log2 mRNA expression (counts per million) in activated $CD4^+$ T cells. G) Rcan3 protein
688 abundance measured by targeted proteomics 24h after activation. $CD28^{-/-}$ (purple), $T^{1792\Delta/\Delta}$
689 (grey), rescue (dark blue), and $T^{1792tg/tg}$ (light blue) are compared to wt (black). Proteins were
690 isolated from the same cells for targeted proteomics of Rcan3 and total RNA sequencing.
691 Numbers indicate p values from t-test. See also supplemental Figure S7.

Data and materials availability:
High-throughput RNA sequencing data will be publically available at GEO accession GSE140568 once published in a peer reviewed journal.

Acknowledgements

We would like to thank the current and former lab members for scientific discussions; Daniel Pinschewer and Weldy Bonilla Pinschewer for advice on LCMV, reagents (GP61 peptide) and scientific discussions; Annaïse Jauch for providing LCMV Armstrong; Mihaela Zavolan and Ed Palmer for deep scientific discussions and critical comments on the manuscript; members of the NCCR RNA & Disease for discussions; the University of Basel, the Basel University Hospital and Department of Biomedicine (DBM) for institutional support; the team from the DBM animal facility for animal husbandry; the DBM flow cytometry core team; Robert Ivanek from the DBM bioinformatics core; Philippe Demougin from the D-BSSE/DBM Genomics Facility Basel; Alexander Schmidt from the University of Basel Biozentrum Proteomics Core Facility for support and Marco Amsler, Caroline Schwenzel, Hélène Rossez, Giuseppina Capoferri and Corinne Engdahl-Démollière for technical assistance. Calculations were performed at sciCORE (http://scicore.unibas.ch/) scientific computing center at University of Basel. This work was supported by grants of the Swiss National Science Foundation (SNSF Professorship PP00P3_144860 to LTJ) and the National Institute Of Allergy And Infectious Diseases of the National Institutes of Health, USA, under Award Number R56/R01AI106923 (to LTJ). The content of this study is solely the responsibility of the authors and does not necessarily represent the official views of the National Institutes of Health.

Author contributions:
M.D. performed and analyzed most experiments; G.B. and C.H. helped to design and interpret metabolic experiments; R.M. provided scientific input, key experimental and infrastructure support; M.K. provided scientific input and experimental support; R.K. generated HITS-CLIP data; D.S. and J.R. performed bioinformatic analysis with the help of J.G.; K.M.A. provided key scientific input and access to HITS-CLIP data; M.D. and L.T.J. designed the experiments, interpreted the data and discussed results; L.T.J. designed the study, obtained funding, supervised all experiments and wrote the manuscript (MS) with the help of M.D.; all authors approved the final MS.

Declaration of interests:
M.D. and L.T.J. are inventors on a patent application related to the findings reported here.

838 **3. References**

839 1 Acuto, O. & Michel, F. CD28-mediated co-stimulation: a quantitative support for
840 TCR signalling. *Nat Rev Immunol* **3**, 939-951, doi:10.1038/nri1248 (2003).
841 2 Esensten, J. H., Helou, Y. A., Chopra, G., Weiss, A. & Bluestone, J. A. CD28
842 Costimulation: From Mechanism to Therapy. *Immunity* **44**, 973-988,
843 doi:10.1016/j.immuni.2016.04.020 (2016).
844 3 Riha, P. & Rudd, C. E. CD28 co-signaling in the adaptive immune response. *Self*
845 *Nonself* **1**, 231-240, doi:10.4161/self.1.3.12968 (2010).
846 4 Linterman, M. A. *et al.* CD28 expression is required after T cell priming for helper
847 T cell responses and protective immunity to infection. *eLife* **3**,
848 doi:10.7554/eLife.03180 (2014).
849 5 Sansom, D. M. & Walker, L. S. CD28 costimulation: walking the immunological
850 tightrope. *Eur J Immunol* **43**, 42-45, doi:10.1002/eji.201243211 (2013).
851 6 Edner, N. M., Carlesso, G., Rush, J. S. & Walker, L. S. K. Targeting co-stimulatory
852 molecules in autoimmune disease. *Nat Rev Drug Discov*, doi:10.1038/s41573-
853 020-0081-9 (2020).
854 7 Leach, D. R., Krummel, M. F. & Allison, J. P. Enhancement of antitumor immunity
855 by CTLA-4 blockade. *Science* **271**, 1734-1736 (1996).
856 8 Kamphorst, A. O. *et al.* Rescue of exhausted CD8 T cells by PD-1-targeted therapies
857 is CD28-dependent. *Science* **355**, 1423-1427, doi:10.1126/science.aaf0683
858 (2017).
859 9 Hui, E. *et al.* T cell costimulatory receptor CD28 is a primary target for PD-1-
860 mediated inhibition. *Science* **355**, 1428-1433, doi:10.1126/science.aaf1292
861 (2017).
862 10 Homet Moreno, B. *et al.* Response to Programmed Cell Death-1 Blockade in a
863 Murine Melanoma Syngeneic Model Requires Costimulation, CD4, and CD8 T Cells.
864 *Cancer Immunol Res* **4**, 845-857, doi:10.1158/2326-6066.CIR-16-0060 (2016).
865 11 Gross, G. & Eshhar, Z. Therapeutic Potential of T Cell Chimeric Antigen Receptors
866 (CARs) in Cancer Treatment: Counteracting Off-Tumor Toxicities for Safe CAR T
867 Cell Therapy. *Annu Rev Pharmacol Toxicol* **56**, 59-83, doi:10.1146/annurev-
868 pharmtox-010814-124844 (2016).
869 12 Martinez-Llordella, M. *et al.* CD28-inducible transcription factor DEC1 is required
870 for efficient autoreactive CD4+ T cell response. *J Exp Med* **210**, 1603-1619,
871 doi:10.1084/jem.20122387 (2013).
872 13 Baumjohann, D. & Ansel, K. M. MicroRNA-mediated regulation of T helper cell
873 differentiation and plasticity. *Nat Rev Immunol* **13**, 666-678, doi:10.1038/nri3494
874 (2013).
875 14 Bartel, D. P. Metazoan MicroRNAs. *Cell* **173**, 20-51, doi:10.1016/j.cell.2018.03.006
876 (2018).
877 15 Loeb, G. B. *et al.* Transcriptome-wide miR-155 Binding Map Reveals Widespread
878 Noncanonical MicroRNA Targeting. *Molecular cell*,
879 doi:10.1016/j.molcel.2012.10.002 (2012).
880 16 Hsin, J. P., Lu, Y., Loeb, G. B., Leslie, C. S. & Rudensky, A. Y. The effect of cellular
881 context on miR-155-mediated gene regulation in four major immune cell types.
882 *Nat Immunol* **19**, 1137-1145, doi:10.1038/s41590-018-0208-x (2018).
883 17 Xiao, C. & Rajewsky, K. MicroRNA control in the immune system: basic principles.
884 *Cell* **136**, 26-36, doi:S0092-8674(08)01633-4 [pii]
885 10.1016/j.cell.2008.12.027 (2009).
886 18 O'Connell, R. M., Rao, D. S., Chaudhuri, A. A. & Baltimore, D. Physiological and
887 pathological roles for microRNAs in the immune system. *Nature reviews.*
888 *Immunology* **10**, 111-122, doi:10.1038/nri2708 (2010).
889 19 Jeker, L. T. & Bluestone, J. A. MicroRNA regulation of T-cell differentiation and
890 function. *Immunological reviews* **253**, 65-81, doi:10.1111/imr.12061 (2013).

20 de Kouchkovsky, D. *et al.* microRNA-17-92 Regulates IL-10 Production by Regulatory T Cells and Control of Experimental Autoimmune Encephalomyelitis. *Journal of immunology* **191**, 1594-1605, doi:10.4049/jimmunol.1203567 (2013).
21 Xiao, C. *et al.* Lymphoproliferative disease and autoimmunity in mice with increased miR-17-92 expression in lymphocytes. *Nat Immunol* **9**, 405-414 (2008).
22 Baumjohann, D. *et al.* The microRNA cluster miR-17 approximately 92 promotes TFH cell differentiation and represses subset-inappropriate gene expression. *Nature immunology* **14**, 840-848, doi:10.1038/ni.2642 (2013).
23 Kang, S. G. *et al.* MicroRNAs of the miR-17 approximately 92 family are critical regulators of T(FH) differentiation. *Nat Immunol* **14**, 849-857, doi:10.1038/ni.2648 (2013).
24 Ferguson, S. E., Han, S., Kelsoe, G. & Thompson, C. B. CD28 is required for germinal center formation. *Journal of immunology* **156**, 4576-4581 (1996).
25 Steiner, D. F. *et al.* MicroRNA-29 regulates T-box transcription factors and interferon-gamma production in helper T cells. *Immunity* **35**, 169-181, doi:10.1016/j.immuni.2011.07.009 (2011).
26 Shahinian, A. *et al.* Differential T cell costimulatory requirements in CD28-deficient mice. *Science* **261**, 609-612 (1993).
27 Shang, W. *et al.* Genome-wide CRISPR screen identifies FAM49B as a key regulator of actin dynamics and T cell activation. *Proc Natl Acad Sci U S A* **115**, E4051-E4060, doi:10.1073/pnas.1801340115 (2018).
28 Linterman, M. A. *et al.* Roquin differentiates the specialized functions of duplicated T cell costimulatory receptor genes CD28 and ICOS. *Immunity* **30**, 228-241, doi:S1074-7613(09)00068-5 [pii]
10.1016/j.immuni.2008.12.015 (2009).
29 Walker, L. S. *et al.* Compromised OX40 function in CD28-deficient mice is linked with failure to develop CXC chemokine receptor 5-positive CD4 cells and germinal centers. *The Journal of experimental medicine* **190**, 1115-1122 (1999).
30 Crotty, S. Follicular helper CD4 T cells (TFH). *Annual review of immunology* **29**, 621-663, doi:10.1146/annurev-immunol-031210-101400 (2011).
31 Gaidatzis, D., Burger, L., Florescu, M. & Stadler, M. B. Analysis of intronic and exonic reads in RNA-seq data characterizes transcriptional and post-transcriptional regulation. *Nat Biotechnol* **33**, 722-729, doi:10.1038/nbt.3269 (2015).
32 Agarwal, V., Bell, G. W., Nam, J. W. & Bartel, D. P. Predicting effective microRNA target sites in mammalian mRNAs. *eLife* **4**, doi:10.7554/eLife.05005 (2015).
33 Gagnon, J. D. *et al.* miR-15/16 Restrain Memory T Cell Differentiation, Cell Cycle, and Survival. *Cell Rep* **28**, 2169-2181 e2164, doi:10.1016/j.celrep.2019.07.064 (2019).
34 Jin, H. Y. *et al.* MicroRNA-17~92 plays a causative role in lymphomagenesis by coordinating multiple oncogenic pathways. *EMBO J* **32**, 2377-2391, doi:10.1038/emboj.2013.178 (2013).
35 Reiley, W. W. *et al.* Deubiquitinating enzyme CYLD negatively regulates the ubiquitin-dependent kinase Tak1 and prevents abnormal T cell responses. *J Exp Med* **204**, 1475-1485, doi:10.1084/jem.20062694 (2007).
36 Mulero, M. C., Aubareda, A., Schluter, A. & Perez-Riba, M. RCAN3, a novel calcineurin inhibitor that down-regulates NFAT-dependent cytokine gene expression. *Biochim Biophys Acta* **1773**, 330-341, doi:10.1016/j.bbamcr.2006.12.007 (2007).
37 Garcia-Alonso, L., Holland, C. H., Ibrahim, M. M., Turei, D. & Saez-Rodriguez, J. Benchmark and integration of resources for the estimation of human transcription factor activities. *Genome Res* **29**, 1363-1375, doi:10.1101/gr.240663.118 (2019).

944 38 Martinez, G. J. *et al.* Cutting Edge: NFAT Transcription Factors Promote the
945 Generation of Follicular Helper T Cells in Response to Acute Viral Infection. *J*
946 *Immunol* **196**, 2015-2019, doi:10.4049/jimmunol.1501841 (2016).
947 39 Vaeth, M. *et al.* Store-Operated Ca(2+) Entry Controls Clonal Expansion of T Cells
948 through Metabolic Reprogramming. *Immunity* **47**, 664-679 e666,
949 doi:10.1016/j.immuni.2017.09.003 (2017).
950 40 Bronevetsky, Y. *et al.* T cell activation induces proteasomal degradation of
951 Argonaute and rapid remodeling of the microRNA repertoire. *The Journal of*
952 *experimental medicine* **210**, 417-432, doi:10.1084/jem.20111717 (2013).
953 41 Wang, C. J. *et al.* CTLA-4 controls follicular helper T-cell differentiation by
954 regulating the strength of CD28 engagement. *Proc Natl Acad Sci U S A* **112**, 524-
955 529, doi:10.1073/pnas.1414576112 (2015).
956 42 O'Donnell, K. A., Wentzel, E. A., Zeller, K. I., Dang, C. V. & Mendell, J. T. c-Myc-
957 regulated microRNAs modulate E2F1 expression. *Nature* **435**, 839-843,
958 doi:10.1038/nature03677 (2005).
959 43 Treiber, T., Treiber, N. & Meister, G. Regulation of microRNA biogenesis and its
960 crosstalk with other cellular pathways. *Nat Rev Mol Cell Biol* **20**, 5-20,
961 doi:10.1038/s41580-018-0059-1 (2019).
962 44 Du, P., Wang, L., Sliz, P. & Gregory, R. I. A Biogenesis Step Upstream of
963 Microprocessor Controls miR-17 approximately 92 Expression. *Cell* **162**, 885-
964 899, doi:10.1016/j.cell.2015.07.008 (2015).
965 45 Bachmaier, K. *et al.* Negative regulation of lymphocyte activation and
966 autoimmunity by the molecular adaptor Cbl-b. *Nature* **403**, 211-216 (2000).
967 46 Chiang, Y. J. *et al.* Cbl-b regulates the CD28 dependence of T-cell activation. *Nature*
968 **403**, 216-220, doi:10.1038/35003235 (2000).
969 47 King, C. G. *et al.* Cutting edge: requirement for TRAF6 in the induction of T cell
970 anergy. *Journal of immunology* **180**, 34-38 (2008).
971 48 Buckler, J. L., Walsh, P. T., Porrett, P. M., Choi, Y. & Turka, L. A. Cutting edge: T cell
972 requirement for CD28 costimulation is due to negative regulation of TCR signals
973 by PTEN. *Journal of immunology* **177**, 4262-4266 (2006).
974 49 Paolino, M. & Penninger, J. M. Cbl-b in T-cell activation. *Semin Immunopathol* **32**,
975 137-148, doi:10.1007/s00281-010-0197-9 (2010).
976 50 Suzuki, A. *et al.* T cell-specific loss of Pten leads to defects in central and peripheral
977 tolerance. *Immunity* **14**, 523-534 (2001).
978 51 King, C. G. *et al.* TRAF6 is a T cell-intrinsic negative regulator required for the
979 maintenance of immune homeostasis. *Nat Med* **12**, 1088-1092, doi:nm1449 [pii]
980 10.1038/nm1449 (2006).
981

Animals

Mice

All animal work was performed in accordance with the federal and cantonal laws of Switzerland. Protocols were approved by the Animal Research Commission of the Canton of Basel-Stadt, Switzerland. Most of the mouse lines were imported from the JAX laboratory as indicated in the key resources table. $T^{1792\Delta/\Delta}$ mice were imported from the laboratory of Dr. Bluestone (UCSF). Rescue SM^{+} mice were obtained by crossing the rescue strain to other transgene lines in house so that their precise genetic origin is difficult to determine. As for the transfer cells, we used SM $CD45.1^{+}$ wt cells imported from SWIMR. All other mouse lines were crossed to CD45.2 expression. Cre negative littermates (from $T^{1792tg/tg}$ or $T^{1792\Delta/\Delta}$) were used as wt controls, and cre negative littermates from the rescue strain were used as CD28ko. 6-8 week old females and males were used for all experiments.

METHOD DETAILS

Organ isolation

Organs were obtained after CO_2 euthanization and kept on ice until processing. Mesenteric lymph nodes (LN), peripheral LN (inguinal, axillary, brachial, six cervical) and spleen were taken for most of the experiments. Spleens were injected with 0.5ml ACK lysis buffer (0.155M NH_4Cl, 200µl 0.5M EDTA pH=8.0, 0.012M $NaHCO_3$ pH 7.2) for erythrolysis before processing. The organs were meshed with 0.4µm filters to obtain single cell suspensions which were then washed with FACS buffer (2% heat-inactivated FCS in PBS, for stainings add 0.02% NaN_3). Cells were centrifuged at 4°C, 5min at a speed of 370g for most washing procedures.

Naïve $CD4^{+}$ T cell isolation

Naïve $CD4^{+}$ T cells were isolated from cell suspensions with pooled lymph nodes and spleen. Isolation was performed with StemCell mouse naïve $CD4^{+}$ T cell isolation kit according to manufacturer's instructions. In brief, the cell suspensions were incubated with rat serum and $CD4^{+}$ isolation antibody for 7.5 minutes, then with memory depletion antibody for 2.5 minutes, and in the end with magnetic beads for another 2.5 minutes before incubating with the isolation magnet for 2.5 minutes. The resulting untouched naïve $CD4^{+}$ T cells were then washed with FACS buffer, and purity was routinely checked with a staining for $CD4^{+}$, $CD44^{-}$ and viability.

Plate-bound $CD4^+$ T cell activation

Plates were coated over night with 0.2µg anti-CD28 and 0.5µg anti-CD3 per ml PBS for most of the experiments (low stimulation as according to [1]). We used 1ml/well for 24 well plates and 0.2ml/well for 96 well plates. Before plating of the cells, plates were washed with PBS. We plated $2*10^5$ naïve $CD4^+$ T cells per well in 96 well flat-bottom in 200µl medium. For 24 well plates, $2*10^6$ naïve $CD4^+$ T cells per ml medium in 1ml medium were plated. Complete T cell medium (RPMI-1640 Medium, 10% FCS, 1% HEPES, 1% non-essential amino acids, 1% Glutamax, 0.1% 2-Mercaptoethanol) was supplied with 50U IL-2/ml. Cells were cultured at 37°C, 5% CO_2 for 24h or longer depending on the purpose of the experiment as indicated in figure legends.

Proliferation assay with cell trace violet (CTV)

Freshly isolated naïve $CD4^+$ T cells were washed with PBS. 1µl of Cell Trace stock solution (dissolved in DMSO according to the manufacturer's instructions) was then used per ml PBS for $10*10^6$ cells. Cells were incubated at 37°C for 20 minutes, then 5x the original staining volume of normal T cell culture medium was added for 5 minutes to remove residual dye. Cells were washed and plated in complete culture medium supplied with 50U IL-2 per ml for 48h.

Enzyme-linked immunosorbent assay (ELISA)

IL-2 secretion was addressed in 48h culture supernatants from cells that were plated in pre-coated wells in complete T cell medium without IL-2. IL-2 ELISA was performed with the BioLegend ELISA MAX mouse IL-2 set according to the manufacturer's instructions. After the last washing step, TMB substrate was added for the readout. Absorbance was measured with an ELISA plate reader (Synergy H1 Hybrid Reader, BioTek) at 450nm as well as 570nm wavelength, and normalized to wild type control samples that were run in the same experiment.

FACS Staining

Generally, cells were stained for viability with viability dye 780 in PBS for 20min at 4°C and then washed with PBS. Non-specific binding was blocked with anti-CD16/anti-CD32 0.5mg/ml on ice for 10 minutes. Surface staining was performed in FACS buffer for 20-30 minutes at 4°C. In intracellular staining or LCMV experiments, cell fixation was performed with Fix-Perm for 20 minutes on 4°C (1h for LCMV experiments). Intracellular staining was done in permeabilization buffer for 1h at 4°C. Activation status of the cells was assessed by staining and gating for singlets/lymphocytes/viable cells/ $CD4^+$ and early activation marker

CD25/CD69 as well as CD44/CD62L expression. Blasting of lymphocytes was addressed by pre-gating on singlets/viable cells. For cytokine staining after *in vitro* differentiation or *ex vivo* e.g., for IL-2 staining, cells were stimulated with 50ng/ml PMA, 500ng/ml Ionomycin and 10 µg/ml Brefeldin A (BFA) for 3h at 37°C before staining. Data was acquired with an LSR Fortessa (BD) and analyzed with FlowJo (version 10.4.1).

LCMV Armstrong infection model

Mice were infected with $2*10^5$ PFU LCMV-Armstrong strain i.p. with U-100 insulin syringes (0.30mm (30G) x 8mm). Eight days post infection, the animals were euthanized with CO_2 and the spleens were harvested for staining. We gated for singlets/lymphocytes/viable cells/$CD3^+CD4^+$ to look at CD44 expression, and moreover we addressed T_{FH} cells by the co-expression of key markers Bcl-6, PD-1, ICOS and CXCR5. We gated for singlets/lymphocytes/viable cells/$CD19^+B220^+$ to look at GC B cells expressing Fas and GL-7. Re-stimulation of splenocytes was performed in flat bottom 96 well plates with 1µg/ml LCMV-specific peptide GP-64 in comparison to polyclonal 50ng/ml PMA, 500ng/ml Ionomycin stimulation for one hour, then 10µg/ml Brefeldin A was added for another three hours before staining. We then gated for T_H1 cells using singlets/lymphocytes/viable cells/$CD3^+CD4^+$ and finally looking at Tbx21/IFNγ expression. All in vivo experiments were performed blinded with assignment of animal numbers after data analysis.

Histology

Spleens were embedded in cryo embedding medium and frozen on dry ice before storage at -80°C. Sections were cut at a thickness of 6µm and dried on air. Single sections were then fixed with acetone for 5 minutes and circled with PAP pen. Staining for CD19, CD4 and GL-7 was performed in FACS buffer with anti-CD16/anti-CD32 in a wet chamber at 4°C overnight. Slides were then washed with PBS on a shaker for 15 minutes before drying and mounting. Imaging was performed with a 20x objective on a Nikon Ti2 microscope and analyzed with ImageJ version 2.0.0.

Adoptive transfer (AT) with subsequent LCMV infection

Naïve $SMARTA^+$ $CD4^+$ T cells from wt, $CD28^{-/-}$ and rescue mice were isolated transferred into $CD28^{-/-}$ recipients. Each recipient received $1*10^5$ cells in 100µl PBS i.v.. The recipients were infected with $2*10^5$ PFU LCMV Armstrong i.p. two days after cell transfer. Eight days after infection, the mesenteric and peripheral LN as well as the spleen were analyzed separately for

the presence of $V\alpha2^+V\beta8.3^+$ T cells (pre-gated on singlets/lymphocytes/viable cells/$CD4^+$), and these cells were further characterized for their CD44 expression. One $CD28^{-/-}$ mouse that did not receive donor cells was used as a negative control in each experiment to display the recipient-intrinsic $V\alpha2^+V\beta8.3^+$ population.

RNA sequencing

For any experiment involving RNA, cells were washed with PBS before counting and the RNA was kept on ice during the experiments, storage at -80°C. All pipetting was performed with filter-tips and RNAse-free tubes. All procedures for the extractions were performed at the facilities with materials, protocols and supervision of the facility experts. For RNA sequencing, $2.5*10^5$ cells were washed with PBS and resuspend in 200µl TRI Reagent. RNA was extracted from Trizol-samples with a Zymo Direct-zol kit which includes DNAse treatment. Quality control was run with a Bioanalyzer. RNA quality was assessed with a Fragment Analyzer (Advanced Analytical) and RNA-seq library preparation was performed using Illumina Truseq stranded kit. Sequencing was performed on an Illumina NexSeq 500 machine to produce single-end 76-mers reads. All steps were performed at the Genomics Facility Basel (ETH Zurich).

Read quality was assessed with the FastQC tool (version 0.11.5). Reads were mapped to the mouse genome (UCSC version mm10) with STAR (version 2.5.2a) [2] with default parameters, except filtering out reads mapping to more than 10 genomic locations (outFilterMultimapNmax=10), reporting only one hit in the final alignment for multimappers (outSAMmultNmax=1) and filtering reads without evidence in the spliced junction table (outFilterType="BySJout").

All subsequent gene expression data analysis was performed using the R software (version 3.5). Read alignment quality was evaluated using the qQCReport function of the R Bioconductor package QuasR (version 1.18). Gene expression was quantified using the qCount function of QuasR [3] as the number of reads (5'ends) overlapping with the exons of each gene assuming an exon union model (using the UCSC knownGenes annotation downloaded on 2015-12-18). To quantify intronic expression levels, exonic coordinates were extended by 10 bp on each side of the exons, and for each gene the resulting read count was subtracted to the read count obtained on the whole gene (extended by 10 bp on each side).

The R Bioconductor package edgeR (version 3.28)[4] was used for differential gene expression analysis. Between samples normalization was done using the TMM method [5]. Only genes with CPM (counts per million reads mapped) values more than 1 in at least 4 samples (the

number of biological replicates) were retained. Principal component analysis (PCA) was performed on the log-transformed normalized CPM values. An generalized linear model including a genotype effect, an activation effect, and a replicate effect (nested within genotype) was fitted to the raw counts (function glmFit), and differential expression was tested using likelihood ratio tests (function glmLRT). P-values were adjusted by controlling the false-discovery rate (Benjamini-Hochberg method) and genes with a FDR lower than 1% were considered differentially expressed.

To select a restricted list of most likely miRNA targets for each seed family, we restricted the genes to those with a conserved 3'UTR seed match (using TargetScan [6]), and a coverage of more than 5 AHC reads. We additionally restricted the list by using differential expression criteria from the first RNA-seq dataset: genes should be significantly differentially expressed between $T^{1792tg/tg}$ and wt, as well as between $T^{1792\Delta/\Delta}$ and wt, with fold-changes in the expected directions; using intronic read counts, genes should not be significantly differentially expressed in the same comparison, at an increased FDR threshold of 10%.

Gene set enrichment analysis was performed with the function camera [7] from the limma package (version 3.42; using the default parameter value of 0.01 for the correlations of genes within gene sets) using gene sets from the curated gene set collection (C2) of the Molecular Signature Database (MSigDB v7.0)[8] with a special focus on gene sets from pathway databases, including KEGG [9], Biocarta (http://cgap.nci.nih.gov/Pathways/BioCarta_Pathways), PID [10] and Reactome [11]. We tested a total of 1,576 gene sets containing more than 10 genes and those with a false discovery rate (FDR) lower than 1% were considered significant.

Regulon enrichment analysis

Regulon enrichment analysis was performed similarly to pathway enrichment analysis using camera from the limma package. DoRothEA v2 regulons [11] were downloaded from https://github.com/saezlab/DoRothEA.

More specifically, we used human TOP10score regulons in VIPER format, containing the targets with the highest quality score possible (and at least 10 genes) per transcription factor. Mouse regulons were obtained by orthology: mouse genes with a 1-to-1 or Many-to-1 relationship to human genes of each DoRothEA regulon were obtained using Ensembl Compara (release 97); only orthology relationships annotated to taxonomic levels "Boreoeutheria", "Eutheria", "Euarchontoglires", "Theria", or "Amniota" were retained. We

tested a total of 1,307 regulons including at least 10 mouse genes and those with a false discovery rate (FDR) lower than 1% were considered significant.

AGO2 HITS-CLIP (AHC) data

Read depths on seed regions of genes targeted by different miRNA seed families were obtained as previously described [12].

In vitro differentiation

T_H1 differentiation conditions were generated with 50U IL-2, 5ng/ml IL-12 and 10µg/ml anti-IL-4 per ml T cell medium [13]. $iT_{reg}s$ were either differentiated with retinoic acid (0.9mM), 250U IL-2, 0.75ng/ml TGFβ, 10µg/ml anti-IFNγ and 10µg/ml anti-IL-4 [14]. T_H17 were generated with 50ng/ml IL-6, 3ng/ml TGFβ, 5µg/ml anti-IFNγ and 10µg/ml anti-IL-4 per ml T cell medium [15]. For the differentiation, $2*10^5$ naïve $CD4^+$ T cells were plated on a pre-coated 96-well flat bottom plate (coated over night with 0.2µg anti-CD28, 0.5µg anti-CD3 per ml PBS) and harvested at 24h, 48h or 72h after plating.

Seahorse

Calibration plates were coated over night with 200µl calibrant. Cell plates were coated with 18µl 0.1M $NaHCO_3$ pH8.0 6.67% CellTak (Seahorse XF96 flux pack, Bucher Biotech, CH). The following day, cell plates were washed with H_2O and left for drying during cell preparation. Compounds were prepared for a final in-well concentration of 1µM for Oligomycin, 2µM for FCCP and 11µM for Rotenone. $CD4^+$ T cells (naïve or activated) were harvested with glucose-free, unbuffered RPMI, washed and counted multiple times before plating $3*10^5$ cells per well. Mitochondrial perturbation was performed by sequential injection of glucose (80mM stock), oligomycin, FCCP and rotenone. Measurements of oxygen consumption rate (OCR, pMoles/min) and extracellular acidification rate (ECAR; mpH/min) were performed with a Seahorse XF96 flux analyzer (Seahorse Bioscience, USA). Data analysis was performed using Prism (Version7.0d), mitochondrial parameters were calculated as described by Gubser et al. [16].

CyA titration

The sensitivity of $CD28^{-/-}$ and rescue cells to compounds interfering with Ca^{2+} signaling was tested. Increasing amounts of CyA were added to the cultures during activation: $2*10^5$ naïve $CD4^+$ T cells were plated in 100µl complete T cell medium in pre-coated 96 well plates. 100µl

of a serial dilution of CyA were then added to result in in-well concentrations of 100ng/ml, 50ng/ml, 25ng/ml, 12.5ng/ml, 6.5ng/ml, 3.125ng/ml, 1.5625ng/ml or 0ng/ml. Cells were then activated in the presence of these CyA concentrations for 48h before harvesting and staining for viability and activation markers.

ImageStream

Naïve $CD4^+$ T cells were isolated and activated for 48h in the presence of 6.25ng/ml CyA. They were then harvested and washed with PBS before fixation for 20min at 4°C. Intracellular staining for NFATc2 was performed in a two-step staining with first 1h at room temperature with anti-NFATc2 in permeabilization buffer, and subsequently 1h at room temperature with goat anti-mouse IgG1 in permeabilization buffer. Nuclei were stained with DAPI in the last 5min of incubation. Acquisition was run on an ImageStreamX Mark2 Imaging flow cytometer (Amnis), and data analysis was performed with the IDEAS software (v6.2).

Reverse transcription (RT) and quantitative PCR (qPCR)

$5*10^5$ cells were washed resuspend in 400µl TRIreagent. RNA isolation was then performed according to the isolation protocol from TRIreagent supplier (SIGMA). In brief, 0.1ml of 1-bromo-3-chloropropane per ml of TRI Reagent was added, samples were mixed by vigorous shaking, incubated for 15min at room temperature and then centrifuged at 12’000g for 15min at 4°C for phase separation. The aqueous phase was then mixed with 0.5 ml of isopropanol per ml of TRI Reagent used, again centrifuged for 10min for RNA precipitation. RNA was then washed with 70% Ethanol and finally resuspend in RNAse-free water. RNA concentration and purity was determined with a Nanodrop2000 Spectrophotometer (ThermoScientific).

Reverse transcription was performed with RNA extracted with TRIzol and the SIGMA MMLV kit on 1µg RNA according to the manufacturer’s instructions. qPCR was run with TaqMan FAST Universal PCR master mix on an Applied Biosystems® Real-Time PCR System. 18S was used as a reference gene.

Proteomics

All procedures for the extractions were performed at the facilities with materials, protocols and supervision of the facility experts. Heavy labeled reference peptides for Rcan3 identification were ordered from JPT (JPT.com, Berlin. Germany). For targeted proteomics, $2.5*10^5$ cells were washed with PBS and pellets were frozen on dry ice until protein extraction. Cells were then lysed in lysis buffer (1% Sodium deoxycholate, 10mM TCEP, 100mM Tris, pH=8.5

adjusted with NaOH/HCl) for 1 minute at 50°C, shaking at 300rpm. Samples were then sonicated (30 sec on, 30 sec off, 10 cycles, Bioruptor, Diagnode) and heated for 10 minutes, 95°C at 300rpm. Chloroacetamide (0.75M) was added to a final concentration of 15mM and the protein samples incubated for 30 minutes at 37°C, shaking at 500rpm. pH was then adjusted to 8-9 using 1M Ammoniumbicarbonate where necessary. Proteins were then digested using Lysin-C (enzyme/protein ratio of 1:200, 37°C for 3h) and trypsin (enzyme/protein ratio of 1:50, 37°C overnight). Peptide samples were then centrifuged at 5000rpm before adding 5% TFA and washing in wash buffer (1% TFA in 2-propanol). Peptides were cleaned up using the Phoenix 96× kit following the vendor protocol (PreOmics, Martinsried, Germany). For LC-MS/MS analysis, peptides were dissolved in LC buffer A (0.15% Formic acid, 2% acetonitrile, shake at 1,400 rpm at 25°C for 5 minutes) to a final peptide concentration of 0.5 µg/µl. iRT-peptides mix was added before analysis.

For LC-MS analysis, parallel reaction-monitoring (PRM) assays [17] were generated from a mixture containing 100 fmol of each heavy reference peptide and shotgun data-dependent acquisition (DDA) LC-MS/MS analysis on a Thermo Orbitrap Fusion Lumos platform (Thermo Fisher Scientific). The setup of the µRPLC-MS system was as described previously [18]. Chromatographic separation of peptides was carried out using an EASY nano-LC 1000 system (Thermo Fisher Scientific), equipped with a heated RP-HPLC column (75 µm x 30 cm) packed in-house with 1.9 µm C18 resin (Reprosil-AQ Pur, Dr. Maisch). Peptides were analyzed per LC-MS/MS run using a linear gradient ranging from 95% solvent A (0.15% formic acid, 2% acetonitrile) and 5% solvent B (98% acetonitrile, 2% water, 0.15% formic acid) to 45% solvent B over 60 minutes at a flow rate of 200 nl/min. Mass spectrometry analysis was performed on Thermo Orbitrap Fusion Lumos mass spectrometer equipped with a nanoelectrospray ion source (both Thermo Fisher Scientific). Each MS1 scan was followed by high-collision-dissociation (HCD) of the 10 most abundant precursor ions with dynamic exclusion for 20 seconds. Total cycle time was approximately 1 s. For MS1, 1e6 ions were accumulated in the Orbitrap cell over a maximum time of 100 ms and scanned at a resolution of 120,000 FWHM (at 200 m/z). MS2 scans were acquired at a target setting of 1e5 ions, accumulation time of 50 ms and a resolution of 30,000 FWHM (at 200 m/z). Singly charged ions and ions with unassigned charge state were excluded from triggering MS2 events. The normalized collision energy was set to 30%, the mass isolation window was set to 1.4 m/z and one microscan was acquired for each spectrum.

The acquired raw-files were database searched against a *Mus musculus* database (Uniprot, download date: 2017/04/18, total of 34,490 entries) by the MaxQuant software (Version

1.0.13.13). The search criteria were set as following: full tryptic specificity was required (cleavage after lysine or arginine residues); 3 missed cleavages were allowed; carbamidomethylation (C) was set as fixed modification; Arg10 (R), Lys8 (K) and oxidation (M) as variable modification. The mass tolerance was set to 10 ppm for precursor ions and 0.02 Da for fragment ions. The best 6 transitions for each peptide were selected automatically using an in-house software tool and imported to SpectroDive (v8.0, Biognosys, Schlieren, Switzerland). A mass isolation lists containing all selected peptide ion masses were exported and imported into the QE-HF operating software for PRM analysis using the same LC and MS setting as above with the following modifications: The resolution of the orbitrap was set to 120k FWHM (at 200 m/z) and the fill time was set to 250 ms to reach a target value of 3e6 ions. Ion isolation window was set to 0.4 Th and the scan range was set to 100-1500 Th. Normalized collision energy was set to 27%. A MS1 scan using the same conditions are for DDA was included in each MS cycle. All raw-files were imported into SpectroDive for protein / peptide quantification. To control for variation in sample amounts, the total ion chromatogram (only comprising peptide ions with two or more charges) of each sample was determined by Progenesis QI (version 2.0, Waters) and used for normalization.

Quantification and statistical analysis

Statistical analysis was performed with GraphPad Prism (v7.0d, Graphpad Software). Normal distribution was not assumed, and non-parametric tests were chosen individually depending on the type of experiment as indicated in the figure legends. The overall statistical significance was set to 5% (α=0.05), and error bars represent standard deviation (SD). N corresponds to number of biological replicates. We used Kruskal-Wallis tests for most of the experiments with more than two unpaired groups and one factor (e.g., %$Fas^{+}GL7^{+}$ population in three genotypes), followed by Dunn's multiple comparison test. We used two-way Anova for experiments including two factors (e.g., %$CD44^{hi}CD62^{lo}$ population in three genotypes activated with or without anti-CD28), followed by Tukey's multiple comparison test.
A *t*-test was used for the analysis of targeted proteomics (each genotype compared to wt).

1. Baumjohann, D., et al., *The microRNA cluster miR-17 approximately 92 promotes TFH cell differentiation and represses subset-inappropriate gene expression.* Nat Immunol, 2013. **14**(8): p. 840-8.

2. Dobin, A., et al., *STAR: ultrafast universal RNA-seq aligner.* Bioinformatics, 2013. **29**(1): p. 15-21.
3. Gaidatzis, D., et al., *QuasR: quantification and annotation of short reads in R.* Bioinformatics, 2015. **31**(7): p. 1130-1132.
4. Robinson, M.D., D.J. McCarthy, and G.K. Smyth, *edgeR: a Bioconductor package for differential expression analysis of digital gene expression data.* Bioinformatics, 2010. **26**(1): p. 139-140.
5. Robinson, M.D. and A. Oshlack, *A scaling normalization method for differential expression analysis of RNA-seq data.* Genome Biol, 2010. **11**(3): p. R25.
6. Friedman, R.C., et al., *Most mammalian mRNAs are conserved targets of microRNAs.* Genome Res, 2009. **19**(1): p. 92-105.
7. Wu, D. and G.K. Smyth, *Camera: a competitive gene set test accounting for inter-gene correlation.* Nucleic Acids Res, 2012. **40**(17): p. e133.
8. Subramanian, A., et al., *Gene set enrichment analysis: A knowledge-based approach for interpreting genome-wide expression profiles.* Proc Natl Acad Sci U S A, 2005. **102**(43): p. 15545-15550.
9. Kanehisa, M., et al., *KEGG: new perspectives on genomes, pathways, diseases and drugs.* Nucleic Acids Res, 2017. **45**(D1): p. D353-D361.
10. Schaefer, C.F., et al., *PID: the Pathway Interaction Database.* Nucleic Acids Res, 2009. **37**(Database issue): p. D674-9.
11. Fabregat, A., et al., *The Reactome Pathway Knowledgebase.* Nucleic Acids Res, 2018. **46**(D1): p. D649-D655.
12. Gagnon, J.D., et al., *miR-15/16 Restrain Memory T Cell Differentiation, Cell Cycle, and Survival.* Cell Rep, 2019. **28**(8): p. 2169-2181 e4.
13. Vigne, S., et al., *IL-36R ligands are potent regulators of dendritic and T cells.* Blood, 2011. **118**(22): p. 5813-23.
14. Barrat, F.J., et al., *In vitro generation of interleukin 10-producing regulatory CD4(+) T cells is induced by immunosuppressive drugs and inhibited by T helper type 1 (Th1)- and Th2-inducing cytokines.* J Exp Med, 2002. **195**(5): p. 603-16.
15. Chen, W.J., et al., *Conversion of peripheral CD4(+)CD25(-) naive T cells to CD4(+)CD25(+) regulatory T cells by TGF-beta induction of transcription factor Foxp3.* Journal of Experimental Medicine, 2003. **198**(12): p. 1875-1886.
16. Gubser, P.M., et al., *Rapid effector function of memory CD8+ T cells requires an immediate-early glycolytic switch.* Nat Immunol, 2013. **14**(10): p. 1064-72.
17. Peterson, A.C., et al., *Parallel reaction monitoring for high resolution and high mass accuracy quantitative, targeted proteomics.* Mol Cell Proteomics, 2012. **11**(11): p. 1475-88.
18. Ahrne, E., et al., *Evaluation and Improvement of Quantification Accuracy in Isobaric Mass Tag-Based Protein Quantification Experiments.* J Proteome Res, 2016. **15**(8): p. 2537-47.